nature communications

Article

https://doi.org/10.1038/s41467-025-57090-4

Prevention of tuberculosis in cynomolgus macaques by an attenuated *Mycobacterium tuberculosis* vaccine candidate

Received: 1 May 2024

Accepted: 11 February 2025

Published online: 25 February 2025

Check for updates

Dhiraj K. Singh[1], Mushtaq Ahmed[2], Sadia Akter[2], Vinay Shivanna[1], Allison N. Bucşan[3], Abhishek Mishra[4], Nadia A. Golden[3], Peter J. Didier[3], Lara A. Doyle[3], Shannan Hall-Ursone[1], Chad J. Roy[3], Garima Arora[1], Edward J. Dick Jr[1], Chinnaswamy Jagannath[4], Smriti Mehra[1,3], Shabaana A. Khader[2] ✉ & Deepak Kaushal[1] ✉

The need for novel vaccination strategies to control tuberculosis (TB) is underscored by the limited and variable efficacy of the currently licensed vaccine, Bacille Calmette-Guerin (BCG). SigH is critical for *Mycobacterium tuberculosis (Mtb)* to mitigate oxidative stress, and in its absence *Mtb* is unable to scavenge host oxidative/nitrosative bursts. The *MtbΔsigH* (*ΔsigH*) isogenic mutant induces signatures of the innate immunity in macrophages and protects rhesus macaques from a lethal *Mtb challenge*. To understand the immune mechanisms of protection via mucosal vaccination with *ΔsigH*, we employed the resistant cynomolgus macaque model; and our results show that *ΔsigH* vaccination significantly protects against lethal *Mtb* challenge in this species. *ΔsigH*-vaccinated macaques are devoid of granulomas and instead generate inducible bronchus associated lymphoid structures, and robust antigen-specific $CD4^+$ and $CD8^+$ T cell responses, driven by a hyper-immune, trained immunity-like phenotype in host macrophages with enhanced antigen presentation. Correlates of protection in *ΔsigH*-vaccinated macaques include gene signatures of T cell activation, IFNG production, including IFN-responsive, activated T cells, concomitant with IFNG production, and suppression of IDO^+ Type I IFN-responsive macrophage recruitment. Thus, *ΔsigH* is a promising lead candidate for further development as an antitubercular vaccine.

Despite impressive gains in the worldwide control of HIV[1], tuberculosis (TB) remains a major global infectious disease of humanity, causing > 1.3 million deaths annually[2]. Although Bacille Calmette-Guerin (BCG) is licensed for TB prevention, its effectiveness against adult pulmonary TB is limited[3]. Novel vaccination strategies are therefore necessary to contain TB. Robust and enduring T cell immunity is imperative to control TB[4]. Due to the absence of major *Mycobacterium tuberculosis* (*Mtb*)-encoded T cell antigens, BCG elicits a narrower range of responses, compared to *Mtb*[5]. Live replicating *Mtb* bacilli with rational attenuation express protective antigens absent from BCG, generating long-lasting immune responses towards a wider antigenic repertoire[6]. One such candidate, MTBVAC *(ΔphoP/ΔfadD26)*, is in advanced human testing[7,8]. Attenuated *Mtb* vaccines devoid of key virulence/detoxification factors hold promise for protecting against TB.

[1]Southwest National Primate Research Center, Texas Biomedical Research Institute, San Antonio, TX, USA. [2]Department of Microbiology, University of Chicago, Chicago, IL, USA. [3]Tulane National Primate Research Center, Tulane University School of Medicine, Covington, LA, USA. [4]Department of Pathology and Genomic Medicine, Houston Methodist Research Institute, Weill-Cornell Medicine, Houston, TX, USA. ✉e-mail: khader@uchicago.edu; dkaushal@txbiomed.org

Oxidative stress is a primary challenge encountered by *Mycobacterium tuberculosis (Mtb)* during its pulmonary pathogenesis. SigH protects *Mtb* against oxidative[9,10] and nitrosative stress[11], heat shock[12], acidic pH[13], phagocytosis[14,15], hypoxia[16] and cell wall disruption[17]. In the absence of SigH, *Mtb* is susceptible to host stress with significantly reduced survival and pathogenicity in lungs[18], even after immunosuppression due to SIV co-infection[19]. Relative to *Mtb*, *ΔsigH*-infected macrophages induce apoptosis and autophagy[20]. Aerosol infection of rhesus macaques with *ΔsigH* results in strong innate immune and adaptive T cell responses, conferring protection against *Mtb*[21].

To unravel the mechanisms underlying the protection conferred by mucosal vaccination with *ΔsigH*, we conducted experiments using the more resistant, cynomolgus macaque species. Our results show that mucosal vaccination with *ΔsigH* recruit T cells expressing IFNG to the airways and lungs, priming an IFNG- rather than a Type I IFN-responsive phenotype in macrophages.

Results

Mucosal ΔsigH is an effective vaccine in cynomolgus macaques

25 cynomolgus macaques underwent challenge with 100 CFU of *Mtb* CDC1551 via aerosol 8 weeks post-vaccination (Fig. 1a), resulting in positive tuberculin skin tests in 17/25 animals. Two unvaccinated, four BCG-vaccinated and two Δ*sigH*-vaccinated CMs did not respond to TST (Table S1). Antigen-specific intracellular cytokine staining (ICS) however confirmed that all CMs that did not respond to TST were positive for *Mtb* infection, mounting robust *Mtb*-specific T cell responses in the lung after challenge, comparable to those from TST-positive macaques (Fig. S1a). Importantly, none of the 25 animals displayed any signs of active infection or disease, such as dyspnea, anorexia, pyrexia or body weight loss (Fig. S1b), perturbation in serum C-reactive protein (CRP) (Fig. S1c), or other peripheral blood attributes associated with the development of TB disease in macaques[22], i.e., A/G (Fig. S1d) and neutrophil/lymphocyte (N/L) (Fig. S1e) ratios, during the vaccination phase. Furthermore, thoracic CXRs obtained post-vaccination for all 16 vaccinated animals were also normal (Fig. S1f). At weeks 3 and 5 post vaccination, bacilli were recovered from more *ΔsigH*- than BCG-vaccinated CMs, indicating that the mutant strain might persist longer than BCG in lungs before being eventually cleared. Seven weeks after vaccination, the levels of *ΔsigH* recovered from BAL were however comparable with BCG (Fig. S1g) ($P = 0.2339$). At this stage, no bacilli could be recovered from 7/9 *ΔsigH*-vaccinated and 7/7 BCG-vaccinated CMs. The number of bacilli recovered from the two *ΔsigH* vaccinated CMs were barely above the lower limit of detection.

After challenge with a high dose of *Mtb* CDC1551, signs of infection, e.g., elevated serum CRP levels (Figs. S1h, i), reduced serum A/G ratios (Fig. 1b), increased frequency (Fig. S1j) and number (Fig. S1k) of neutrophils and elevated blood N/L ratios (Fig. 1c) were observed in unvaccinated CMs. In comparison, animals in the two vaccinated groups exhibited significantly lower serum peak and endpoint CRP levels (Figs. S1h, i) and significantly higher A/G ratios (Fig. 1b). While neutrophil levels decreased in both vaccinated groups relative to unvaccinated animals, the reduction in the BCG- but not the *ΔsigH*- vaccinated groups was significant (Figs. 1c, Fig. S1j, k). Significantly more granuloma involvement was observed after *Mtb* challenge in the unvaccinated, relative to the vaccinated groups by the analysis of CXR scans (Fig. 1d).

Elite protection by mucosal vaccination with ΔsigH relative to BCG

Significantly lower *Mtb* CFUs were recovered from the BALs of *ΔsigH*-vaccinated animals relative to unvaccinated and BCG-vaccinated macaques, at 3, 5 and 7 weeks after *Mtb* challenge (weeks 11, 13 and 15 post-vaccination) (Fig. 1e), as well as at the at the endpoint (Fig. S1l). While the difference between the unvaccinated and the BCG-vaccinated CMs was significant at weeks 3 and 5 time-points ($P = 0.0005$, week 3; $P = 0.00052$, week 5), that between unvaccinated and *ΔsigH*-vaccinated, and more importantly between BCG- and *ΔsigH*-vaccinated CMs was highly statistically significant at these times ($P < 0.0001$ for all comparisons, two-way ANOVA with Tukey's multiple comparison correction). Significantly reduced *Mtb* burdens were also obtained from the lungs, lung-derived granulomas, lung-draining bronchial lymph nodes (BrLN), spleen, liver and kidneys (Figs. 1f–h, Fig. S1m–o) of *ΔsigH*-vaccinated macaques, relative to the two other groups. Thus, the lung *Mtb* burden in CMs vaccinated with *ΔsigH* was >four-logs lower than in unvaccinated ($P < 0.0001$), and ~three-logs lower than in BCG-vaccinated ($P < 0.0001$) animals. In comparison, mucosal BCG vaccination resulted in a significant ($P = 0.0049$), but smaller (~1-log) reduction in lung bacillary burden compared to the unvaccinated group (Fig. 1f). Bacilli could be recovered from lesions obtained from only 1/9 *ΔsigH* vaccinated macaques but were present in granulomas isolated from 9/9 unvaccinated and 5/7 BCG vaccinated animals. The mean CFU burden in the lung granulomas for *ΔsigH*-vaccinated CMs was three-logs lower ($P < 0.0001$) than unvaccinated and two-logs lower ($P < 0.0001$) than BCG-vaccinated animals (Fig. 1g). *ΔsigH* vaccination caused BrLNs to be sterile, with 5-logs lower *Mtb* burdens than unvaccinated macaques (Fig. 1h). Extrapulmonary sites - spleen, liver and kidneys—of *ΔsigH* vaccinated animals were sterile, while significantly higher (2-3-logs) *Mtb* burdens were present in that of unvaccinated or BCG-vaccinated macaques (Figs. S1m–o). Vaccination with *ΔsigH* resulted in a significantly greater frequency (>75%) of lung lobes to be sterile (i.e., devoid of culturable *Mtb*), relative to BCG-vaccinated (~25%) or unvaccinated (0%) macaques (Fig. S1p). These results are supported by the analysis of CXR scans at the endpoint which show significantly lower granulomatous pathology in the vaccinated, relative to the other two groups (Fig. 1d).

Vaccination with ΔsigH led to reduced lung pathology

Gross pathology analysis at necropsy demonstrated greater involvement in granulomatous and inflammatory pathology in the lungs of unvaccinated animals (Fig. 1i) relative to BCG-vaccinated (Fig. 1j) and *ΔsigH*-vaccinated (Fig. 1k) animals. Sub-gross histopathology analysis revealed that animals vaccinated with both *ΔsigH* (Fig. 1n) and BCG (Fig. 1m) had significantly fewer lung lesions, as well as reduced oedema, pneumonia, and generalized foci of inflammation upon challenge with *Mtb*, relative to unvaccinated CMs (Fig. 1l). Morphometric quantification of lung pathology showed that both the BCG- (Fig. 1p) and *ΔsigH*-vaccinated (Fig. 1q) groups had significantly lower pathology ($P < 0.0001$) compared to unvaccinated animals (Fig. 1o), with no detectable difference between the two vaccinated groups (Fig. 1r). The frequency of cellular inflammation (Fig. 1s) and necrosis (Fig. 1t) in the lung sections of unvaccinated CMs was also significantly higher than both vaccinated groups. The lungs of unvaccinated CMs were heavily involved in granulomatous pathology (Fig. 1o), consistent with a mean >15% lung pathology score (Fig. 1r). Most of these lesions were highly circumscribed, confluent, and centrally necrotic (Fig. 1o). Non-necrotic lesions were occasionally present in the vicinity of larger necrotic lesions in this group. Vaccinated macaques were characterized by a greater degree of normal lung space and smaller granulomas (Fig. 1m, n, p, q). BCG-vaccinated CMs harbored non-necrotic lesions more frequently than unvaccinated controls (Fig. 1m, p). The lungs of all but one *ΔsigH* vaccinated macaques did not harbor any granulomas. The lung lesions observed in the few *ΔsigH* vaccinated CMs, were non-necrotic, with abundant lymphoid follicles (Fig. 1n, q). Lung sections from *ΔsigH* vaccinated CMs had a significantly greater frequency of lymphoid follicles in the lungs (Fig. 1u). Lymphoid follicles - iBALT (inducible bronchus-associated lymphoid tissue)—are critical for protection from TB induced by *ΔsigH*[23].

Characterization of post Mtb challenge immune responses

The frequencies of T cell populations ($CD3^+$, $CD4^+$ and $CD8^+$) and B cells were indistinguishable in the BAL of all three groups after *Mtb*

https://doi.org/10.1038/s41467-025-57090-4

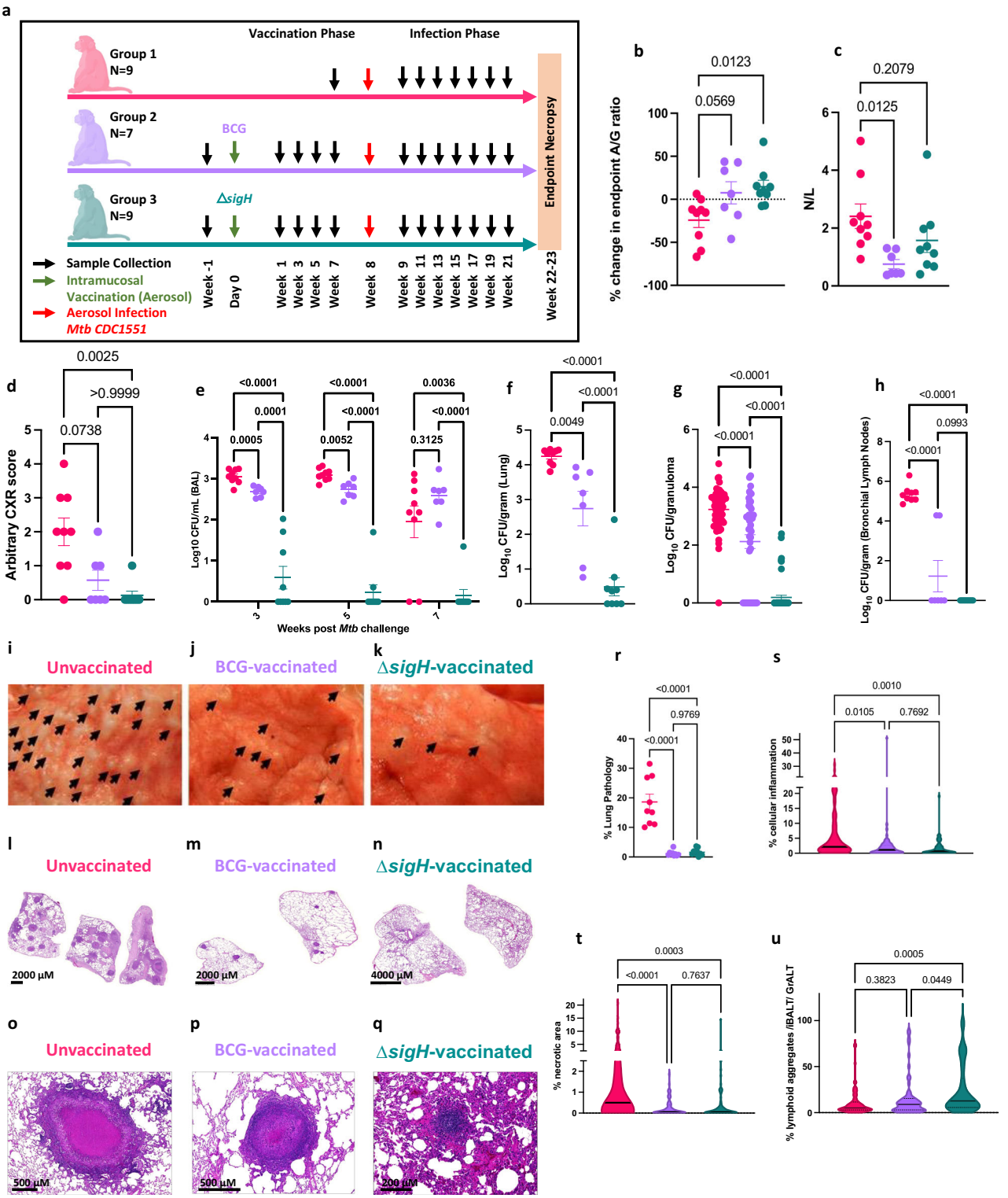

Fig. 1 | *ΔsigH* vaccination protects from TB disease. a Experimental design. In unvaccinated (strawberry), BCG (lavender) and *ΔsigH*-vaccinated (teal) CMs post-*Mtb* infection. The schematics were created using BioRender. Shown are endpoint serum Albumin/Globulin (A/G) ratios (**b**); blood Neutrophil (N)/Lymphocyte (L) ratios (**c**) and CXR scores (**d**); longitudinal BAL Colony Forming Units (CFUs) (**e**); endpoint lung (**f**), lung granuloma (**g**), and bronchial lymph node (**h**) CFUs per gram. Gross pathology in representative unvaccinated (**i**), BCG- (**j**) and *ΔsigH*-vaccinated (**k**) with granulomas (black arrows). Representative sub-gross histopathology and histopathology of unvaccinated (**l**, **o**), BCG- (**m**, **p**) and *ΔsigH*-vaccinated (**n**, **q**) CM lungs. Unvaccinated: Multiple confluent necrotic granulomas (**o**), BCG-vaccinated: (**p**) and *ΔsigH* -vaccinated: Solitary non-necrotic small granuloma with lymphoid hyperplasia and iBALT (**q**). Morphometric lung pathology score in the three groups (**r**). Percentage of cellular inflammation (**s**), necrotic region (**t**) and lymphoid aggregates (**u**), across multiple fields of view of lung tissue using HALO (Indica Labs). Data is presented as mean ± standard error of mean (SEM) and *P*-values were calculated by one-way ANOVA with Tukey's correction, except for (**d**) where a two-way ANOVA with Tukey's correction was used.

https://doi.org/10.1038/s41467-025-57090-4

challenge across multiple timepoints (Fig. S2a–d). Lung-homing ($CCR5^+$) phenotype was significantly elevated in *ΔsigH*-vaccinated animals (Fig. S2e–g). The frequencies of $Ki67^+$ T cells were higher in the BAL of *ΔsigH*-vaccinated animals at week 3. No changes were detected in the frequencies of effector, memory or naïve $CD4^+$ or $CD8^+$ T cells in BAL post *Mtb* challenge (Fig. S2h–m). Antigen-specific $CD4^+$ and $CD8^+$ T cell populations did not express significantly different levels of IFNG, TNF-α, GZMB or IL17 in responses to *Mtb* Cell-wall (CW) (Fig. S2r-y).

Vaccination with ΔsigH induces strong T cell responses in the BAL

Significantly greater absolute numbers as well as frequencies of $CD3^+$ (Figs. 2a, Fig. S3a), $CD4^+$ (Figs. 2b, Fig. S3b) and $CD8^+$ (Figs. 2c, Fig. S3c) T cells and B cells (Figs. 2d, Fig. S3d) were present in the airways of *ΔsigH*- relative to BCG vaccinated CMs, showing peak at week 3 post vaccination and followed by a gradual decline over time. A vast majority of $CD3^+$ (Figs. 2e, Fig. S3e), $CD4^+$ (Figs. 2f, Fig. S3f), and $CD8^+$ (Figs. 2g, Fig. S3g) T cells and B cells (Figs. 2h, Fig. S3h) exhibited lung

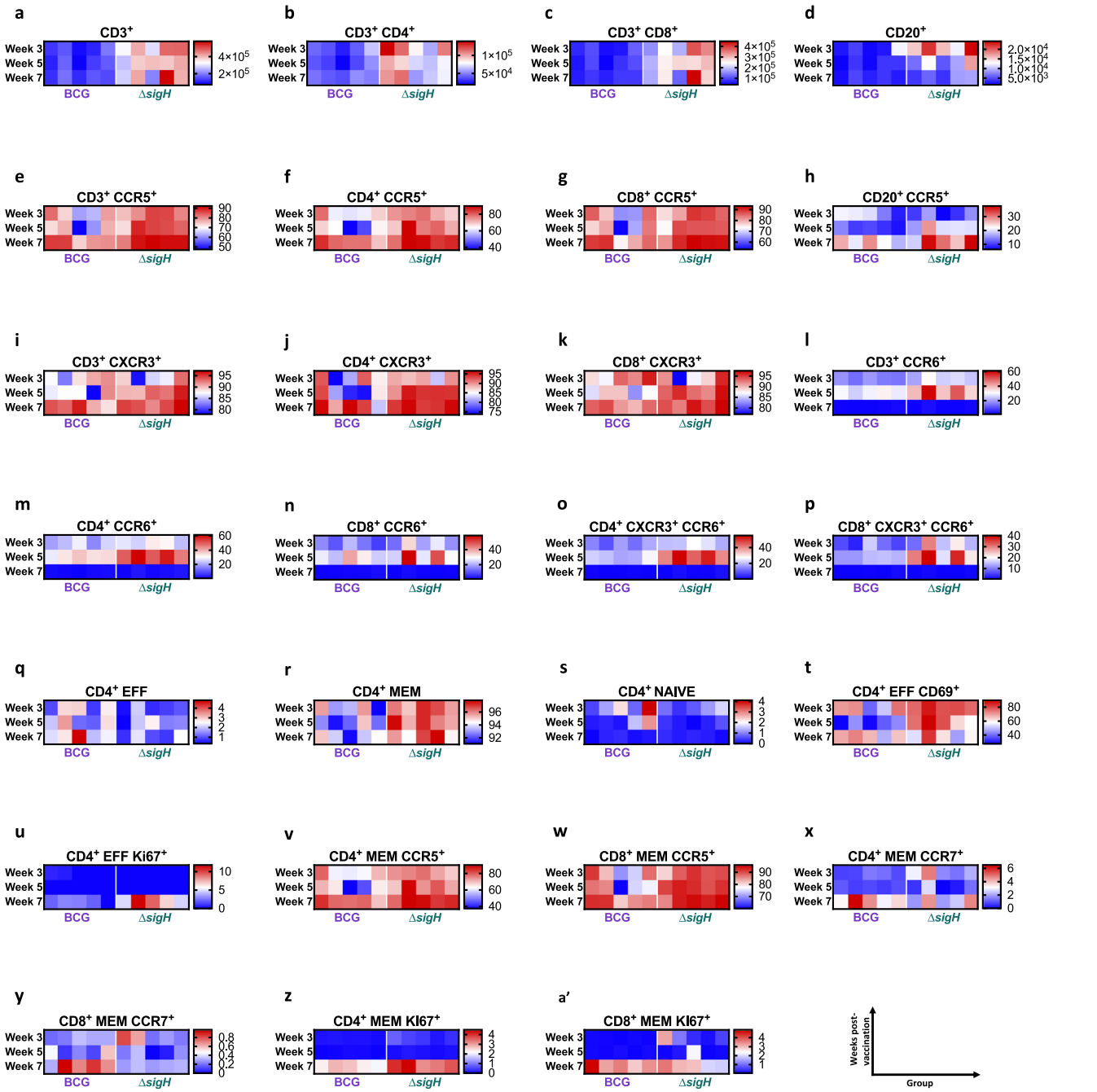

Fig. 2 | *ΔsigH* promotes lymphocytic immune responses in BAL post-vaccination. Absolute counts of $CD3^+$ (**a**), $CD4^+$ (**b**), and $CD8^+$ (**c**) T cells and B cells (**d**), in BAL at weeks 3, 5, and 7 post-vaccination time-point in BCG- (lavender) or *ΔsigH*- (teal) vaccinated CMs. Each column represents an individual macaque ($n = 5$). Frequencies of $CCR5^+$ and $CXCR3^+$ - $CD3^+$ (**e**, i), $CD4^+$ (**f**, **j**), and $CD8^+$ (**g**, **k**) T cells and B cells (**h**) in BAL. Frequencies of $CCR6^+$ $CD3^+$ (**l**), $CD4^+$ (**m**) and $CD8^+$ (**n**) T cells in BAL. Frequencies of $CXCR3^+CCR6^+$ $CD4^+$ (**o**) and $CD8^+$ T cells in BAL (**p**); effector (**q**), memory (**r**) and naïve (**s**) $CD4^+$ T cells, $CD69^+$ (**t**) and $KI67^+$ (**u**) effector $CD4^+$ T cells, $CCR5^+$ (**v**), $CCR7^+$ (**x**) and $KI67^+$(**z**) memory $CD4^+$ T cells and $CCR5^+$ (**w**), $CCR7^+$ (**y**) and $KI67^+$(**a'**) memory $CD8^+$ T cells in BAL at weeks 3, 5, and 7 post-vaccination time-point, expressed as percentage of parental population. Results are shown for weeks 3, 5, and 7 post-vaccination time-point ($n = 5$). Each column represents an individual macaque.

homing phenotype ($CCR5^+$), with higher frequencies post-vaccination in the BAL of *ΔsigH*- relative to BCG vaccinated CMs which increased over time; indicating that a superior immune response was elicited by *ΔsigH* vaccination. This was accompanied by relatively much lower frequencies of $CCR7^+$ $CD3^+$ (Fig. S4a), $CD4^+$ (Fig. S4b) and $CD8^+$ (Fig. S4c) T and B cells (Fig. S4d). In all T cell populations *ΔsigH*- relative to BCG vaccination resulted in increased early SLO homing marker expression in the $CD4^+$ compartment (indicative of iBALT formation) (Fig. S4b). *ΔsigH* vaccination also resulted in the significantly greater recruitment of Th1 - $CXCR3^+/CD3^+$ (Figs. 2i, Fig. S3i), $CD4^+$ (Figs. 2j, Fig. S3j), $CD8^+$ (Figs. 2k, Fig. S3k), Th17 - $CCR6^+/CD3^+$ (Figs. 2l, Fig. S3l), $CD4^+$ (Figs. 2m, Fig. S3m) and $CD8^+$ (Figs. 2n, Fig. S3n) and Th1/Th17 (Th*) - $CXCR3^+CCR6^+$/ $CD4^+$ (Figs. 2o, Fig. S3o) and $CD8^+$ (Figs. 2p, Fig. S3p) T cells to the BAL. CXCR3 expression in T cells increased over time, while CCR6 expression showed a peak at week 5 and declined at week 7. The frequencies of $CD69^+$ (activated) $CD3^+$ (Fig. S4e), $CD4^+$ (Fig. S4f), and $CD8^+$ (Fig. S4g) T cells and B cells (Fig. S4h) were not impacted by vaccination. Fewer $CD3^+$ (Fig. S4i), $CD4^+$ (Fig. S4j), and $CD8^+$ (Fig. S4k) T cells and B cells (Fig. S4l) displayed proliferative ($Ki67^+$) phenotype, significantly higher frequencies were generally observed for the *ΔsigH*- relative to BCG vaccinated CMs. The frequencies of BAL $CD3^+$ (Fig. S4m), $CD4^+$ (Fig. S4n) and $CD8^+$ (Fig. S4o)/ HLA-DR^+ T cells were lower than the $CD69^+$ subpopulations with no significant differences in the two vaccination groups. The overwhelming majority of $CD4^+$ T cells in the BAL were memory cells (>90%) and their frequency was significantly increased by *ΔsigH*-, relative to BCG-vaccination (Fig. 2r, Fig. S3r) across multiple timepoints. In contrast, significant changes were not observed for effector/ naïve subpopulations after *ΔsigH*-, relative to BCG-vaccination (Fig. 2q, s, Fig. S3q, s). The memory phenotype distribution was different for $CD8^+$ T cells–with 20–40% exhibiting effector and 60-80% memory phenotype with very few naïve cells. Most effector $CD4^+$ (Fig. 2t, Fig. S3t) and $CD8^+$ (Fig. S4p) T cells were $CD69^+$, and the frequency of the $CD4^+CD69^+$ subpopulation (Fig. 2t, Fig. S3t) increased significantly after *ΔsigH*-, relative to BCG-vaccination. Fewer effector $CD4^+$ (Figs. 2u, Fig. S3u) and $CD8^+$ (Fig. S4q) T cells were $Ki67^+$ than $CD69^+$, but the frequency of the $CD4^+Ki67^+$ subpopulation increased after *ΔsigH*-, relative to BCG-vaccination (Fig. 2u, Fig. S3u). In the memory $CD4^+$ and $CD8^+$ T cell subpopulations, $CCR5^+$ (Figs. 2v, w, Fig. S3v, w), $CCR7^+$ (Figs. 2x, y, Fig. S3x, y) and $Ki67^+$ (Figs. 2z, a', Fig. S3z, a') phenotypes increased significantly, while $CD69^+$ did not, (Figs. S4r, s) after *ΔsigH*-, relative to BCG-vaccination. Thus, the frequencies of effector and memory $CD4^+/CD8^+$ T cells were significantly altered in the BAL by *ΔsigH*, relative to BCG-vaccinated CMs.

Strong airway T cell responses after ΔsigH vaccination are antigen-specific

$CD4^+$ T cells in the BAL of *ΔsigH*-vaccinated CMs expressed significantly higher levels of IFNG, upon recall stimulation with CW (Figs. 3a, Fig. S5a) or EC (Figs. 3k, Fig. S6a), at multiple-to-all timepoints analyzed. The peak levels of antigen specific $CD4^+$, IFNG responses in the BAL to *ΔsigH* vaccination were in the range of 20–30% for CW and 8–10% for EC, much higher than unstimulated (2–5%) (Fig. S6b) but lower than positive controls (40–50%) (Fig. S6c). In general, CW (Fig. 3, Fig. S5) generated responses with larger magnitude than EC (Figs. 3, Fig. S6) in our hands, indicating a wider antigenic repertoire of the *ΔsigH* induced T cell responses. $CD4^+$ T cells in the BAL of *ΔsigH*-vaccinated CMs also expressed significantly higher levels of TNF-α at all time-points studied upon recall stimulation with CW (Figs. 3b, Fig. S5b) and at different time-points upon stimulation with EC (Figs. 3l, Fig. S6d). The simultaneous expression levels of IFNG/TNF-α in response to CW (Figs. 3c, Fig. S5c) and EC (Figs. 3m, Fig. S6e) was also significantly higher in the BAL from *ΔsigH*- relative to BCG-vaccinated macaques. Significantly higher expression of GZMB was observed on $CD4^+$ T cells after stimulation with CW (Figs. 3d, Fig. S5d), while differences approached statistical significance between the two groups upon stimulation with EC (Figs. 3n, Fig. S6f). Significantly higher frequency of $CD4^+$ T cells in the BAL of *ΔsigH*- relative to BCG-vaccinated macaques also expressed IL17 during the early week 3 but not the later time-points upon stimulation with CW (Figs. 3e, Fig. S5e), but not EC (Figs. 3o, Fig. S6g). Comparable results were obtained for antigen specific $CD8^+$ T cells - significantly higher frequency of $CD8^+$ T cells in the BAL of *ΔsigH*- relative to BCG-vaccinated macaques expressed IFNG (Figs. 3f, Fig. S5f, Fig. 3p, Fig. S6h), TNF-α(Figs. 3g, Fig. S5g, Fig. 3q, Fig. S6i), or both (Figs. 3h, Fig. S5h, Fig. 3r, Fig S6o), upon recall stimulation with CW or EC at some-to-all timepoints analyzed. Differences upon stimulation of $CD8^+$ T cells for GZMB and IL-17 expression with either CW (Figs. 3i, j, Fig. S6j, l) or EC (Figs. 3s, t, S6k, m) were not statistically different between the two groups. Aerosol vaccination of CMs with *ΔsigH* therefore, not only induces significantly higher *Mtb*-specific $CD4^+$ T cell responses, but additionally also induces strong antigen-specific $CD8^+$ T cell responses, resulting in enhanced antigen specific wide-spectrum cytokine expression.

In-depth characterization of post-vaccination responses in the airways

We compared responses in BAL at pre-vaccination baseline (Group 1) to 3 weeks post-vaccination in BCG- and *ΔsigH* vaccinated (Groups 2, 3), unvaccinated/3 weeks post *Mtb* challenge (Group 4) and BCG- and *ΔsigH* vaccinated/3 weeks post-*Mtb* challenge (Groups 5, 6) by scRNAseq (Fig. S7a). We identified 20 major populations of cells in BAL (Fig. S7b), including 13 of myeloid and four of lymphoid origin. Due to the significant induction of B and T cell responses in the BAL of *ΔsigH* vaccinated CMs (Figs. 2–3, Figs. S3–6), we focused our analyzes on these cells. The 10 different clusters of lymphocytes (identified by reclustering) included: two $CD4^+$ T cell (C0, C3), three CD8-NK cell - $CD8a^+$/NK (C1), $CD8b^+$/NK (C2) and $CD8ab^+$-NK (C4), T cell doublets (C5), T cells expressing proliferation markers (C6), B cells (C7), γδ T cells (C8) and T cells expressing IFN response markers (C9) (Fig. 4a–c). Significantly higher frequencies of clusters C1 (Fig. 4e), C2 (Fig. 4f), C6 (Fig. 4j), C7 (Fig. 4k) and C9 (Fig. 4m) were present in the BAL of *ΔsigH*- (Group 3), relative to BCG-vaccinated (Group 2) macaques (Fig. 4d–m). Supervised hierarchical clustering of the top genes expressed in each of these clusters (Fig. 5a), across samples, revealed the different states that lymphocytes exist in the airways. C0 expressed Th1, T cell effector function, activation, trafficking, apoptosis genes (KLRB1, CD2, LTB, LCK, CD52 and CRIP and TSPO) at significantly higher levels in *ΔsigH*-vaccinated, relative to BCG-vaccinated samples (Figs. 5a, b, Supplementary data 1). C1 expressed cytolysis, lysosomal processing and T cell development[24] genes (GZMB, CTSD and CD74 at significantly higher levels in *ΔsigH*-vaccinated, relative to BCG-vaccinated samples (Figs. 5a, c, Supplementary data 1). The expression of cytolytic markers GZMA, GZMB, GZMK, PRF1, KLRK1, KLRB1, KLRD1, CTSB, CTSD and NKG7 was induced in C2 (Fig. 5a, d) to significantly higher levels in the BAL of *ΔsigH*- compared to BCG-vaccinated animals (Figs. 5d, Supplementary data 1). The genes significantly induced in the BAL of *ΔsigH* relative to BCG vaccinated CMs in C6 (Figs. 5e, Supplementary data 1) included ACTG1 (required for T cell activation/proliferation). The expression of IRF family transcription factor, IRF-8, induced by IFNG, was strongly expressed to higher levels in the B cell cluster, C7 (Fig. 5f, Supplementary data 1), in the BAL of *ΔsigH*- relative to BCG-vaccinated CMs. IRF8 governs B cell lineage development and activation and their organization into B cell follicles. Other characteristics of C7 included induced expression of BLK (BCR signaling and development), BANK1 (B-T cell cross talk), CD74 (B cell proliferation, migration and adhesion), CD79B (B cell antigen), HLA-DRA (B cell activation), IGHM (IgM isotype), MEF2C, MS4A1 and TCF4 (B cell proliferation, germinal center development). Mucosal vaccination with *ΔsigH* induces significantly higher levels of B cell follicles. Depletion of B cells led to inferior activation of lung T cells and

https://doi.org/10.1038/s41467-025-57090-4

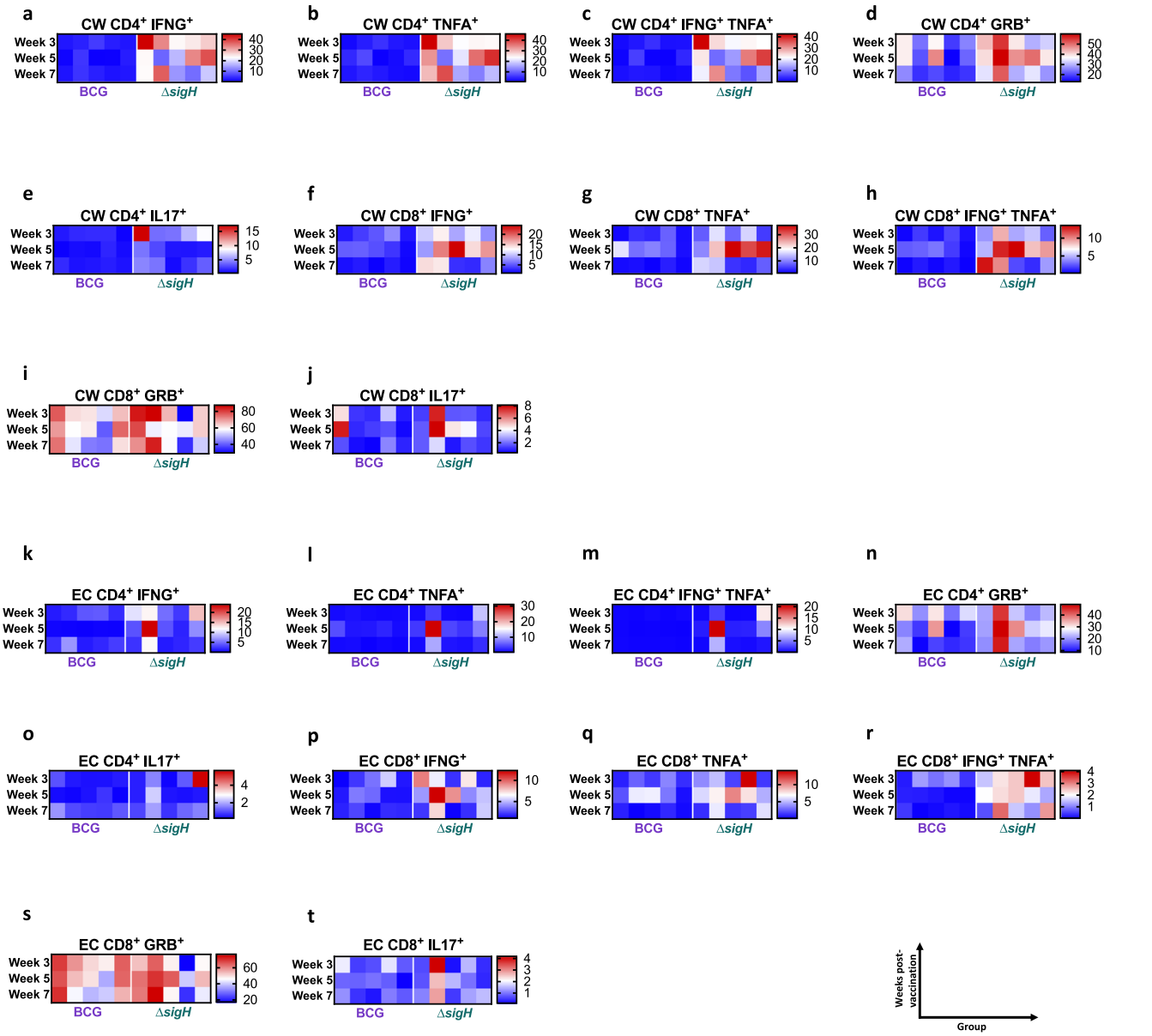

Fig. 3 | *ΔsigH* vaccination induces superior antigen-specific responses in BAL post-vaccination. Frequencies of CD4$^+$ and CD8$^+$ T cells expressing Interferon-γ (IFNG) (**a**, **f**), Tumor Necrosis Factor-α (TNFA) (**b**, **g**), IFNG and TNFA (**c**, **h**), Granzyme-B (GZMB) (**d**, **i**) and Interleukin-17 (IL17) (**e**, **j**) in response to *Mtb* Cell-Wall (CW) fraction in CMs vaccinated with BCG (lavender) or *ΔsigH* (teal) are shown. Frequencies of CD4$^+$ and CD8$^+$ T cells expressing IFNG (**k**, **p**), TNFA (**l**, **q**), IFNG and TNFA (**m**, **r**), GZMB (**n**, **s**) and IL17 (**o**, **t**) in response to pooled peptide pools of *Mtb* ESAT6 and CFP10 (EC). Each column represents an individual macaque ($n = 5$) at weeks 3, 5, and 7 post-vaccination.

reversed *ΔsigH*-induced vaccine protection in RMs[23]. The strong impact of IFNG stimulation was best observed in cluster C9, where IFN-responsive T cells (T-IFNs)[25] were present in significantly higher frequency in *ΔsigH*- relative to BCG-vaccinated BAL samples (Figs. 4m), and expressed higher levels of IFIT3, IFI6, ISG15, OAS2, HERC6, MX1, MX2, HERC5, IFIT5, IRF2, IRF7, IRF9 and ISG15 (Fig. 5g). ISG15, a small ubiquitin-like modifier (SUMO) which targets many proteins for degradation and ultimately inhibits the Type I IFN response[26], while IFIT5 also negatively regulates Type I IFN. Type I-IFNs and IFNG are critical for establishing cell-autonomous antimicrobial immunity, but the latter functions predominantly as a macrophage-activating cytokine[27]. Type I IFN responses require STAT1 transcription, while Th1 responses promoted by IFNG are driven via STAT1 phosphorylation. Accordingly, the expression of STAT1, and the frequency of cells expressing it, were lower in the BAL of *ΔsigH*-, relative to BCG-vaccinated CMs (Fig. 5g). *ΔsigH* vaccination therefore caused the recruitment of lung-homing, Th1/Th1 + Th17 T cells to the lung (Figs. 2, Fig. S3–4), which express IFNG in an antigen-specific manner (Figs. 3, Figs. S5–6). This resulted in IFNG mediated regulation of the T cell response after *ΔsigH* vaccination. Significantly greater interaction score was obtained for interactions between C9 and C1 (Fig. S7g), C9 and C6 (Fig. S7h) and C9 and C7 (Fig. S7i) after *ΔsigH* vaccination as compared to cognate interactions after BCG vaccination (Fig. S7d–f). Thus, *ΔsigH* vaccination not only invokes a significantly higher level of IFNG-expressing CD4$^+$ T cell response, but also CD8$^+$ T cell/cytolytic response, suggesting altered antigen-presentation by vaccination with this mutant via the mucosal route. Our results identify a strong impact of antigen-specific IFNG expression leading to T cells maturation to an activated, IFN-responsive T cell state, which results in enhanced T cell – B cell cooperation and stronger cytolytic T cell responses in the lungs.

Acute *Mtb* infection leading to TB disease strongly induces Type I IFN expression in pDCs[28]. This in turn leads to Type I IFN-priming of

https://doi.org/10.1038/s41467-025-57090-4

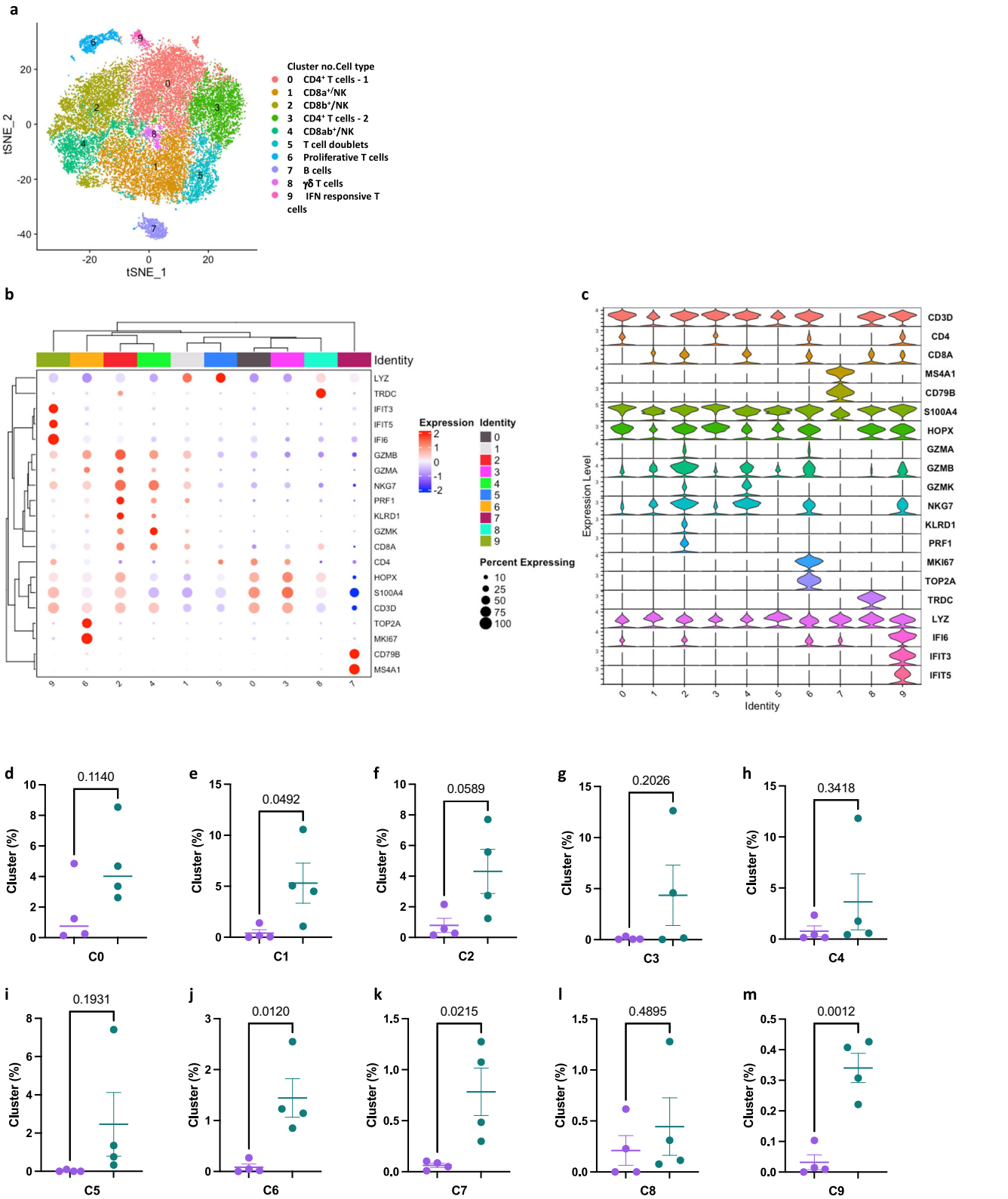

Fig. 4 | scRNAseq in BAL cells reveals lymphocytic enrichment. a tSNE visualization of re-clustered lymphocytes (all conditions together). **b** Bubble plot and **c**. violin plot depicting expression of canonical marker genes used for identification of lymphocyte populations. **d**–**m** Comparison of nine identified lymphocyte clusters between the BCG (lavender) or *ΔsigH* (teal) -vaccinated groups showing cluster 0 (**d**), cluster 1 (**e**), cluster 2 (**f**), cluster 3 (**g**), cluster 4 (**h**), cluster 5 (**i**), cluster 6 (**j**), cluster 7 (**k**), cluster 8 (**l**), and cluster 9 (**m**). Data is presented as mean ± SEM and *P*-values are derived from Mann-Whitney U test.

macrophages to express high levels of immunoregulatory molecules, e.g., IDO[28]. IDO is a potent immunoregulator expressed at very high levels in NHP[29] and TB human[30] granulomas on Mac-IFNs and mediates suppression of anti-TB T cell activities[31]. Within myeloid clusters (Fig. 6a–c), the Mac-IFN cluster (C9, expressing IFI27, ISG15 and IFI6) (Fig. 6d) had a lower frequency of IDO⁺ cells, in the BAL of *ΔsigH*-relative to BCG-vaccinated macaques. The expression of several ISGs, including TYMP, IFIT5, IFIT3, IFIT2, IFI6, GBP2 and CXCL10 occurred to

https://doi.org/10.1038/s41467-025-57090-4

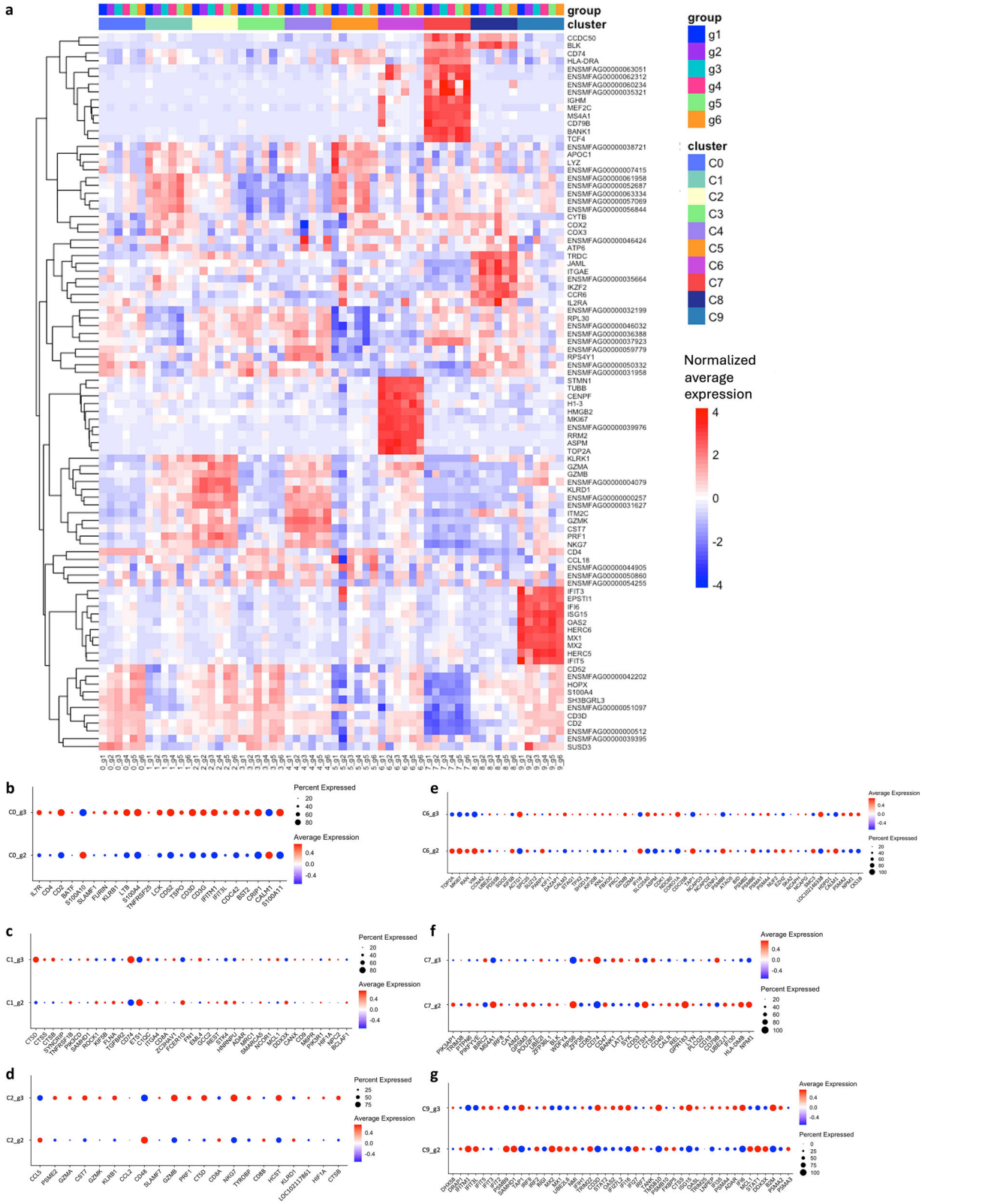

Fig. 5 | scRNAseq - hierarchical cluster and detailed analysis of individual lymphocyte clusters with significant differences between the BCG- and *ΔsigH*-vaccinated groups. a Hierarchical clustering of top genes from the nine clusters identified as lymphocytes. **b**–**g** Bubble plots highlighting six key lymphocyte clusters (C0, C1, C2, C6, C7, C9) show the expression of selected significant markers within each cluster, illustrating differences in expression levels between the BCG (lavender) or *ΔsigH* (teal)–vaccination groups three weeks post-vaccination. The color of each dot indicates the normalized expression level, while the dot size represents the percentage of cells within that cluster expressing the corresponding gene. To identify cluster-specific markers, we compared the gene expressions of each cluster against all other clusters combined using Wilcoxon rank-sum tests, with Bonferroni correction for multiple hypothesis testing with adjusted *p*-value threshold of 0.05.

https://doi.org/10.1038/s41467-025-57090-4

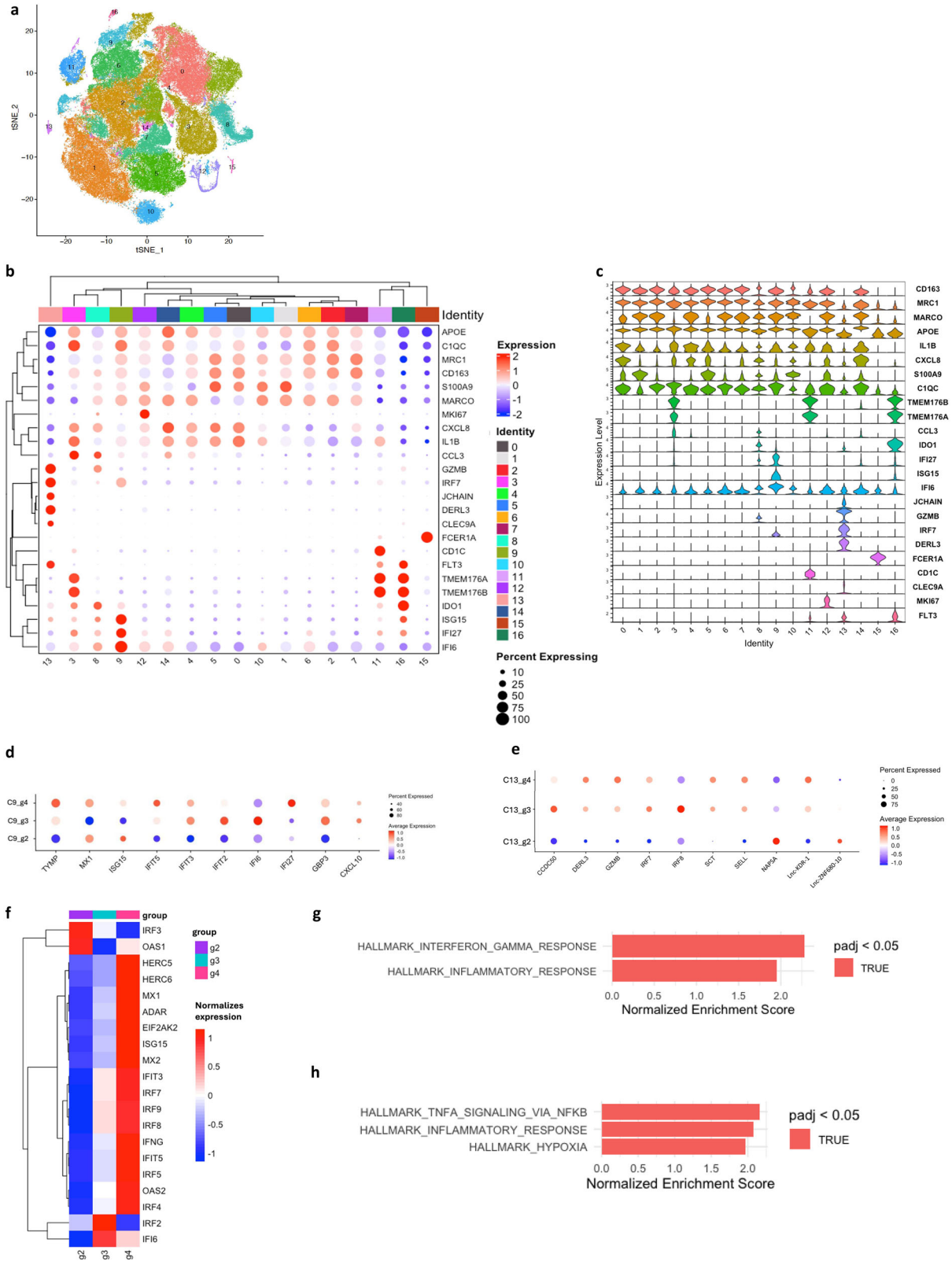

a higher level and in a greater frequency of cells in the BAL of *ΔsigH* (Group 3), relative to BCG-vaccinated (Group 2) macaques (Fig. 6d). This response was driven by T cell generated IFNG, as pDCs after *ΔsigH* vaccination expressed comparable levels of Type I IFN signature relative to BCG vaccination (C13) (Fig. 6e). While the overall expression of ISGs was most highly induced by *Mtb* infection at week 3 (Group 4), *ΔsigH* vaccination (Group 3) resulted in higher expression than BCG vaccination (Group 2) (Figs. 6f, Fig. S7c). The pathways, genes for which were enriched the 3-week *Mtb* infection relative to the comparable *ΔsigH* vaccination time-point included TNFA Response (Fig. 6h). However, when comparing the two vaccination groups at week 3, IFNG Response was one of two pathways enriched after *ΔsigH* vaccination (Fig. 6g). Hence, our results show that vaccination with *ΔsigH* results in significantly greater induction of IFNG from T cells,

Fig. 6 | scRNAseq - hierarchical cluster and analysis of individual myeloid clusters with significant differences between the BCG- and *ΔsigH*-vaccinated groups. a tSNE visualization of reclustered myeloid cells (all conditions together). **b** Bubble plot and (**c**) violin plot depicting expression of canonical marker genes used for identification of myeloid cell populations. **d**–**e** Bubble plots focused on two key myeloid clusters, Mac-IFN and pDCs, show the expression of selected significant markers within each cluster, highlighting differences in expression levels across various groups. Cluster-specific markers were identified using Wilcoxon rank-sum tests, with Bonferroni correction for multiple hypothesis testing. Parameters: only.pos = TRUE, min.pct = 0.25, logfc.threshold = 0.25. **f** Expression of IFN-related genes across groups. **g**–**h** Significant Hallmark pathways showing differences in Mac-IFN cluster between groups 3 vs 2 (**g**) and groups 3 vs 4 (**h**) in cluster Mac-IFN. Pathway analyzes are based on permutation test for independence from the fgsea R package using the Molecular Signatures Database (MSigDB) for human hallmark gene sets. Benjamini-Hochberg corrections for multiple hypothesis testing with FDR < 0.05.

leading to a balanced IFNG/Type I IFN response in the lungs, correlating with elite control of *Mtb* infection. BCG vaccination on the other hand, fails to induce broad IFN responses (IFNG from T cells and Type I IFN from pDCs), while pathogenic *Mtb* infection results in unbalanced expression of Type I IFN signaling from pDCs. During active pulmonary TB, IDO expression in the lung compartment is limited primarily to a subset of interstitial macrophages (Mac-IFNs)[28]. IDO expression in the lungs of *ΔsigH* infected lungs is significantly lower than during active TB[32], and the frequency of Mac-IFNs is significantly lower in *ΔsigH*-vaccination relative to *Mtb* infection at week 3. Expression of IDO is known to occur on DCs in many other contexts, including in lung granulomas formed in infections other than TB, e.g., *L. monocytogenes*. However, the expression of IDO was not detected on DCs in active TB[28]. Here, we detected that maximal IDO expression in BAL occurred on a DC cell cluster (Cluster 16) that expressed TMEM176A-B$^+$/, required by DCs for optimal antigen-presentation to T cells[33], particularly cross-presentation required for MHC I/CD8$^+$ T cell responses and for the inhibition of inflammasome activation. These cation ion channel transporters are expressed on Type 3 DCs (cDC3s), localized in endosomes and phagosomes and are critical for their acidification. Phagosomal acidification is a critical bacterial control mechanism, but *Mtb* is known to subvert it in a redox stress response-dependent manner[34], including via SigH expression[13]. These results suggest that *ΔsigH* may be processed differentially by the phagosomal system compared to *Mtb*.

Comparison of the phenotype of ΔsigH and Mtb in human macrophages (HMΦs)

Since our data suggested that *ΔsigH* was differentially processed by host macrophages, we sought to investigate its immunogenicity in IFNG-activated host macrophages (HMΦs), which not only phagocytose and harbor *Mtb* but can present mycobacterial antigens to CD4$^+$ and CD8$^+$ T cells enabling anti-TB immunity[35,36]. Growth profiles in HMΦs confirmed the highly attenuated phenotype of *ΔsigH* compared to *Mtb (*Fig. 7a). We used RNAseq to dissect the immune responses of HMΦs to *Mtb* CDC1551 and *ΔsigH*[37]. Gene expression data analyzed using Reactome and KEGG workflow[38] showed that unlike *Mtb*, *ΔsigH* induced up-regulation of genes associated with Antigen Processing and ER-Phagosome sorting in addition to many other pro-inflammatory gene modules consistent with mediating anti-TB immunity (Fig. 7b–c*)*. Thus, the expression of antigen processing genes ATG5 (Fig. 7d) and ATG7 (Fig. 7e) was induced to significantly higher levels in the cells infected with *ΔsigH*, relative to *Mtb*. Interestingly, the expression of IFNG-stimulated genes GBP1 (Fig. 7f) and GBP2 (Fig. 7g) was also induced in *ΔsigH*, relative to *Mtb*-infected macrophages. Immunogenicity of whole cell TB vaccines depends on their ability to induce antigen presenting cells like MΦs to secrete Th1 type cytokines, degrade in phago-lysosomes and present peptide epitopes to T cells in vitro[39–41]. Since *ΔsigH*-infection led to an enrichment of antigen processing, ER-phagosome modules and *ATG* genes in MΦs compared to *Mtb* CDC1511 (Fig. 7b–g), we determined whether *ΔsigH* induces autophagy in MΦs and enhances antigen presentation. Confocal image analysis indicated that significantly more *ΔsigH* colocalized with the ATG8/LC3 autophagy marker than *Mtb* CDC1511 (Fig. 7h, i). We have earlier optimized an ex vivo assay where murine and human APCs infected with BCG or *Mtb* rapidly present Ag85B derived epitopes to CD4 T cells specific for Ag85B[42]. In this assay, *ΔsigH* infected MΦs showed a robust Ag85B epitope presentation to F9A6 CD4 T cells (Fig. 7j). Importantly, siRNA knockdown of beclin1, a key autophagy initiator reduced antigen presentation (Fig. 7k). Because *ΔsigH* upregulates *ATGs* in MΦs (Fig. 7b–h), we suggest that it is a hyper-immunogenic mutant in human MΦs with an ability to activate cytokine secretion, autophagy and enhancing antigen processing. These results provide a rationale for the excellent protection shown by *ΔsigH*, and the mechanism by which superior T cell responses are elicited by its vaccination.

Analysis of granuloma-specific immune responses post-challenge

ΔsigH vaccination protects against lethal TB challenge by recruiting IFNG expressing CD4$^+$ and cytolytic CD8$^+$ T cells to the lungs, while limiting the pathogenic impact of Type I IFN primed macrophages. We specifically compared immune responses in dematricized granulomas to understand the impact of vaccination on their function. The frequency of CD4$^+$ T cells within lung granulomas was significantly higher in the *ΔsigH* vaccinated, compared to either unvaccinated, or BCG-vaccinated group (Fig. 8a). The frequency of naïve CD4$^+$ T cells was significantly lower in *ΔsigH*-, relative to BCG-vaccinated lung granulomas (Fig. 8b). The granulomas of *ΔsigH*-vaccinated group harbored a greater frequency of memory CD4$^+$ T cells, relative to the BCG-vaccinated group (Fig. 8c). Within the memory CD4$^+$ T cell pool, significantly greater frequency of activated (CD69$^+$) cells were present in the *ΔsigH*-, relative to the BCG-vaccinated group (Fig. 8d). The proliferative capacity was comparable across the vaccinated groups, but significantly lower than unvaccinated macaques (Fig. 8e), indicating that the lower *Mtb* burdens in the lung granulomas after *ΔsigH* vaccination create the generation of a CD4$^+$ memory pool with an activated-but a non-proliferative profile. Within the effector pool, again the frequency of activated (CD69$^+$) CD4$^+$ T cells was significantly higher after *ΔsigH*, relative to the BCG-vaccination (Fig. 8f), although the activation levels were the highest in the unvaccinated CMs, likely reflecting the greater antigenic burden in that group. Within the parental CD4$^+$ T cell pool as well, the frequency of activated (CD69$^+$) T cells were higher after *ΔsigH* vaccination relative to the other two groups (Fig. 8g), despite several logs lower *Mtb* burdens in the lungs, indicating superior activation of T cell responses by vaccination with the mutant strain. While the frequencies of CD8$^+$, and naïve CD8$^+$ T cells were significantly lower in the *ΔsigH*- relative to the BCG-vaccinated group (Fig. 8h, i), the CD8$^+$ memory pool and activation was significantly higher after *ΔsigH*, relative to BCG vaccination (Fig. 8j, k). Within this fraction, significantly higher frequencies of activated (Fig. 8l) and comparatively higher but statistically non-significant lung homing (CCR5$^+$) (Fig. 8m) cells were also present after *ΔsigH*-, relative to BCG-vaccination. Similarly, within the effector CD8$^+$ T cell pool, significantly higher frequencies of activated (Fig. 8n) cells were also present after *ΔsigH*-, relative to BCG vaccination. These results show the elite level of T cells responses elicited by *ΔsigH* vaccination compared to BCG. Furthermore, significantly higher frequencies of B cells (Fig. 8o) with CD69$^+$ (Fig. 8p) and CCR5$^+$ (Fig. 8q) phenotype were present in granulomas obtained from *ΔsigH*- relative to the BCG-

https://doi.org/10.1038/s41467-025-57090-4

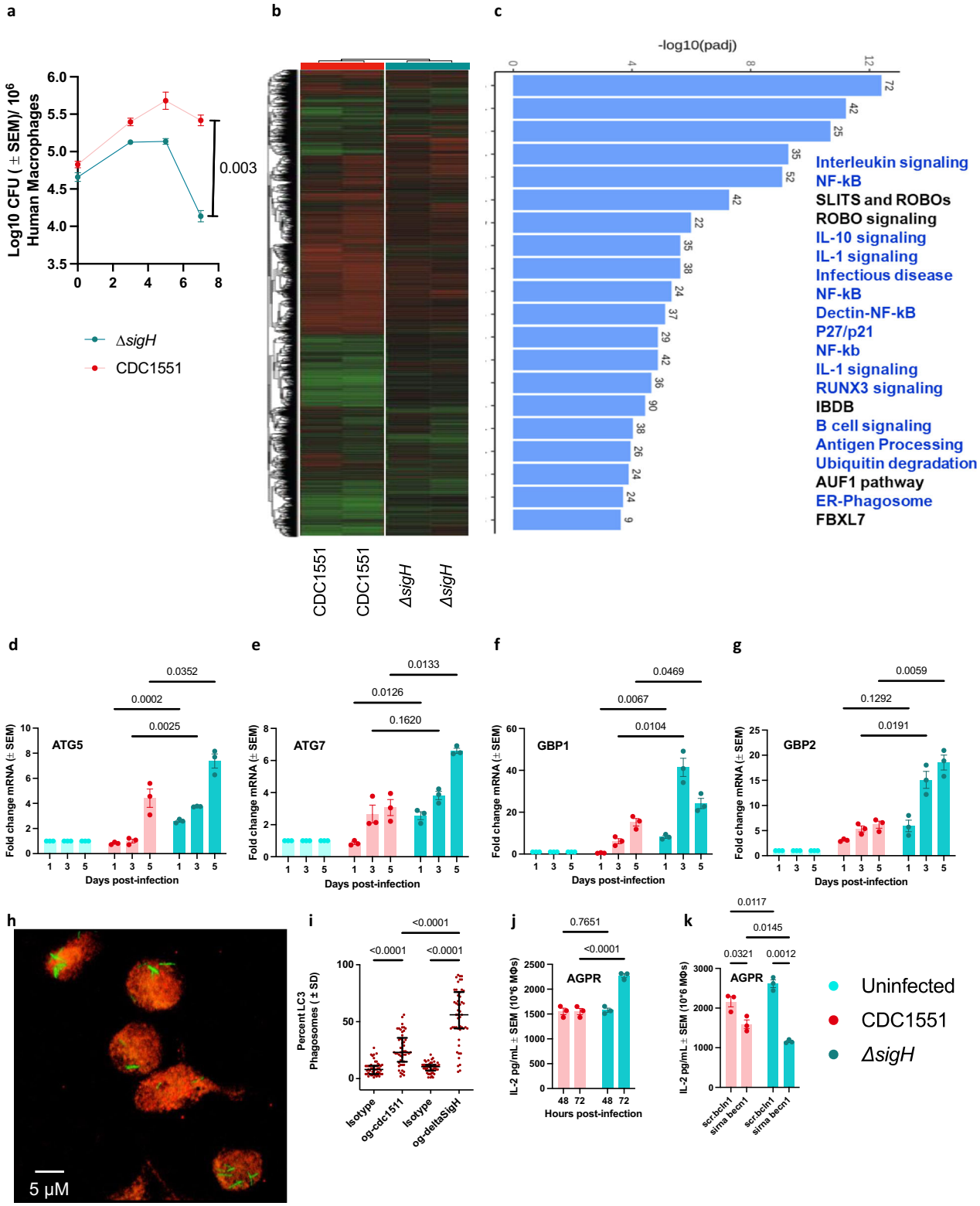

vaccinated group. Granuloma derived B cells in both the vaccinated groups displayed comparable proliferative capacity which was significantly lower than unvaccinated groups (Fig. 8r). To further understand the differences between protective and permissive granulomas from the lungs of macaques, we employed the cyclic immunofluorescence (CyCIF) multilabel spatial biology staining (Akoya Biosciences) (Fig. 9). Representative lung sections from unvaccinated, BCG-vaccinated and *ΔsigH*-vaccinated macaques each, were studied using a panel of 27 protein markers (Fig. S9a–b), antibody staining for which were either already validated or optimized specifically for this study (Fig. S8a, Table S3). We focused our analyzes on unvaccinated- (as a representative of progressive, high *Mtb* burden containing granulomas) and *ΔsigH* vaccinated- (as a representative of protective, low *Mtb* burden containing granulomas) sections. Using Akoya's proprietary StarDist nuclear segmentation on DAPI staining, we identified 891,314 single cells in unvaccinated- (Fig. S9c-f) and 646,055 in *ΔsigH* vaccinated sections (Figs. S9g–j). The lung section from the unvaccinated macaque was characterized by granulomas with extensive

Fig. 7 | *ΔsigH* is hyperimmunogenic and upregulates genes associated with anti-TB immunity in human macrophages. CD14 bead purified human macrophages (HMΦs) were pooled from two donors and three pools were infected with *ΔsigH* (teal) and CDC1551 *Mtb* (red) (MOI = 1) for 4 hours. **a** On days indicated HMΦs were lysed and plated for CFU counts on 7H11 agar. **b**–**c** Two pools ($n = 3$ M and $n = 3$ F each) of donor derived HMΦs were infected as above and subjected to RNAseq at 18 hours post infection (Novogene USA). Heatmaps show fragments per kilobase million (FPKM). Data were analyzed using Reactome and Kyoto encyclopedia of genes and Genomes (KEGG) workflows followed by GSEA analysis. Reactome analysis of *ΔsigH* induced genes vs. those induced by *Mtb* shown and enriched gene modules are highlighted. TRIzol lysates of preparations from panel-a were used for RT-PCR analysis using primers (Table S4) for *ATG5* (**d**), *ATG7* (**e**), *GBP1* (**f**), GBP2 (**g**) genes. Uninfected samples are shown in turquoise. **h**–**i** Oregon green labeled live *ΔsigH* and *Mtb* were phagocytosed into HMΦs followed by immunofluorescent labeling using monoclonal antibody (mab) to microtubule associated loath chain-3 biomarker of autophagosomes (red) or isotype. Colocalization was acquired using an N90 Nikon fitted with Metaview software. Fifty HMΦs in triplicates per organism were counted blind for colocalizing phagosomes and averaged from two independent experiments. **j** Three pools ($n = 2$/pool) of HLA-DR1+ HMΦs were infected with *ΔsigH* and *Mtb* (MOI = 1) washed, and one set lysed immediately to plate for CFU counts. Replicate set was overlaid using (1:1) F9A6 CD4$^+$ T cell hybridoma that secretes IL-2 upon recognition of Ag85B derived peptide epitope. IL-2 in the supernatant collected at 48 and 72 hours post overlay was measured using sandwich ELISA. **k** Replicate antigen presentation assay was done using HLA-DR1+ HMΦs in which beclin1 has been knocked down 24 hours earlier using a siRNA probe (Origene, USA). Data is presented as mean ± SEM and *P*-values are derived from multiple Mann-Whitney tests (one-way) with multiple hypothesis correction by false discovery rate method of Benjamini, Kreiger and Yekutielli (two stage step up).

central necrosis, and higher frequency of myeloid cells in the rim adjoining the necrotic area (Fig. 9a, b). These granulomas were not only positive for high levels of CD68, CD163, CD206 and IDO, but also for IDO$^+$ cells that did not express any of the above myeloid markers (Fig. 9c). We attribute this signal, which was only present in the unvaccinated sample, to MDSCs, which we have earlier shown to express IDO in the context of *Mtb* infection but which are lineage negative cells[43]. The lung section from the *ΔsigH* vaccinated macaque was characterized by granulomas with limited necrosis and significant iBALT (Fig. 9d–f). Intensely CD20, CD19 and CD21 (all B cell markers) positive iBALT from these lung samples were organized in B cell and T cell zones akin to LNs. In fact, significant colocalization correlation was observed between B cell markers PAX5, CD20, CD21, CD19 with each other and this correlation was much stronger in the *ΔsigH* vaccinated, protected (Fig. 9i), relative to the unvaccinated, permissive (Fig. 9g) granulomas. The expression of CD3e, CD4, and CD8 was most strongly correlated with ICOS, FoxP3, CD45 and HLA-A in the vaccinated section (Fig. 9i). On the contrary, the correlation between B cell and T cell markers was reduced in the unvaccinated sample (Fig. 9g). 29 different phenotypes were identified in the unvaccinated section (Fig. 9h), while 27 phenotypes were identified in the *ΔsigH*-vaccinated section (Fig. 9j). The two additional phenotypes in the unvaccinated sample (Fig. 9h) included an abundant cell type – unidentified IDO$^+$ cells which are likely MDSCs. The expression of CCR2 correlated with SMA, suggesting that CCR2/CCL2 are required for the interaction between macrophages and smooth muscle cells to initiate and amplify the migration and proliferation of the latter, during inflammation[44]. In protective granulomas from *ΔsigH* vaccinated CMs, the most prominent module was the B cell module (Fig. 9i), which was present in B cells as well as proliferating B cells, again highlighting the strong B cell follicle response generated by *ΔsigH*; followed by the T cell module which was present in both ICOS$^+$- T helper and T cytotoxic cell populations in the lung granulomas. Other T cell populations such as helper and cytotoxic T cells, or proliferating- helper and cytotoxic T cells, or granzyme B$^+$ - helper and cytotoxic T cells, or CCR2$^+$- helper and cytotoxic T cells were positive for markers CD3e, CD4, CD8, HLA-A, CD45 and ICOS and exhibited greater correlation in the *ΔsigH* vaccinated (Fig. 9i) compared to unvaccinated (Fig. 9g) samples. Greater frequency of cytotoxic (Fig. 9k) and helper T cells (Fig. 9l) as well as proliferating B cells (Fig. 9m) were present in the lungs of *ΔsigH* vaccinated compared to unvaccinated samples, by CyCIF. Many T cell populations (helper and cytotoxic T cells, or proliferating-, granzyme B$^+$-, or CCR2$^+$- or helper and cytotoxic T cells) clustered with endothelial cells, proliferating endothelial cells and CD31$^+$PCK$^+$ endothelial cells. CD31 (PECAM-1) is an efficient signaling molecule mainly distributed in vascular endothelial cells, is negatively correlated with lung injury[45]and has diverse roles in angiogenesis, platelet function, apoptosis, thrombosis, mechanosensing of endothelial cell response to fluid shear stress, and negative regulation of multiple stages of leukocyte migration through venular walls[46], including monocytes, neutrophils[47] and NK cells[48]. The inhibition of neutrophil recruitment by CD31 is mediated by IFNG[49], which we have shown is highly induced in *ΔsigH*-vaccinated lungs. Overall, in the granulomas of *ΔsigH* vaccinated macaques, two of the largest cellular populations were CD31$^+$ - (30%) and CD31$^-$ - endothelial cells (28%) (Fig. S9a, b). The two important myeloid cell populations which clustered together were CD163$^+$/CD68$^+$/CD206$^+$/Vimentin$^+$ alveolar macrophages and CD163$^+$/CD68$^+$/Vimentin$^+$/IDO$^+$ macrophages, while two other populations, M2 macrophages (CD163$^+$/CD68$^+$) and less well characterized macrophages (CD68$^+$) clustered away from this module. Next, we performed neighborhood analysis to identify which subpopulations of cells interacted with which others. 20 cellular neighborhoods were identified in the granulomas of *ΔsigH* vaccinated macaques (Fig. 9n, o, S9c, d). CD31$^+$ endothelial cells and endothelial cells formed neighborhoods with many other cellular subpopulations due to their higher frequency. CD31$^+$ endothelial cells associated with epithelial cells, other endothelial cells and proliferative endothelial cells. These cells also associated with cytotoxic T cells. B cells primarily associated with T helper cells. Since we have previously identified B cell follicles as involved in *ΔsigH* vaccination induced protection from TB in RMs, we studied if greater B cell follicles were present in *ΔsigH* vaccinated, relative to unvaccinated CMs as well. Comparatively more B cell populations (B cells, proliferative B cells) were present in the lungs of *ΔsigH* vaccinated (Fig. 9o, S9f), relative to unvaccinated CMs (Figs. 9n, S9e). These cells organized in iBALT to a comparatively greater extent (Fig. 9o, S9f). On the contrary, the permissive granulomas from unvaccinated/*Mtb* infected CMs were characterized by greater influx of myeloid cells (Fig. 9a) including IDO$^+$ MDSCs (Fig. 9c). The frequency of cells staining for structural markers, e.g., smooth muscles, epithelial and endothelial cells was greater in the unvaccinated relative to *ΔsigH* vaccinated lungs. We identified that most cells in a macaque TB granuloma were of non-immunocytic origin. Increased frequencies of structural cells are likely associated with greater granuloma formation in the unvaccinated group. Interestingly, the one structural cell population which was more frequent in the *ΔsigH* vaccinated lung was pCK$^+$CD31$^+$ (Fig. 9h).

Discussion

BCG, the only vaccine licensed for the prevention of TB, has recently been shown to induce impressive immune responses and protection in macaques via the intravenous route of vaccination[4]. Intradermal vaccination with BCG, however, is unable to protect globally against adult pulmonary TB[5]. Furthermore, BCG is not safe in individuals with HIV infection and is particularly contraindicated in infants with HIV[50]. Clearly, novel anti-tubercular vaccines beyond BCG are needed to save millions of human lives. Ideally, the new vaccine(s) will be safe, immunogenic and highly effective (in the range of > 75% protection from disease). Candidates to replace BCG include DNA[51], subunit[52], viral[53] and whole-cell live (recombinant BCG or attenuated *Mtb*)[54]

https://doi.org/10.1038/s41467-025-57090-4

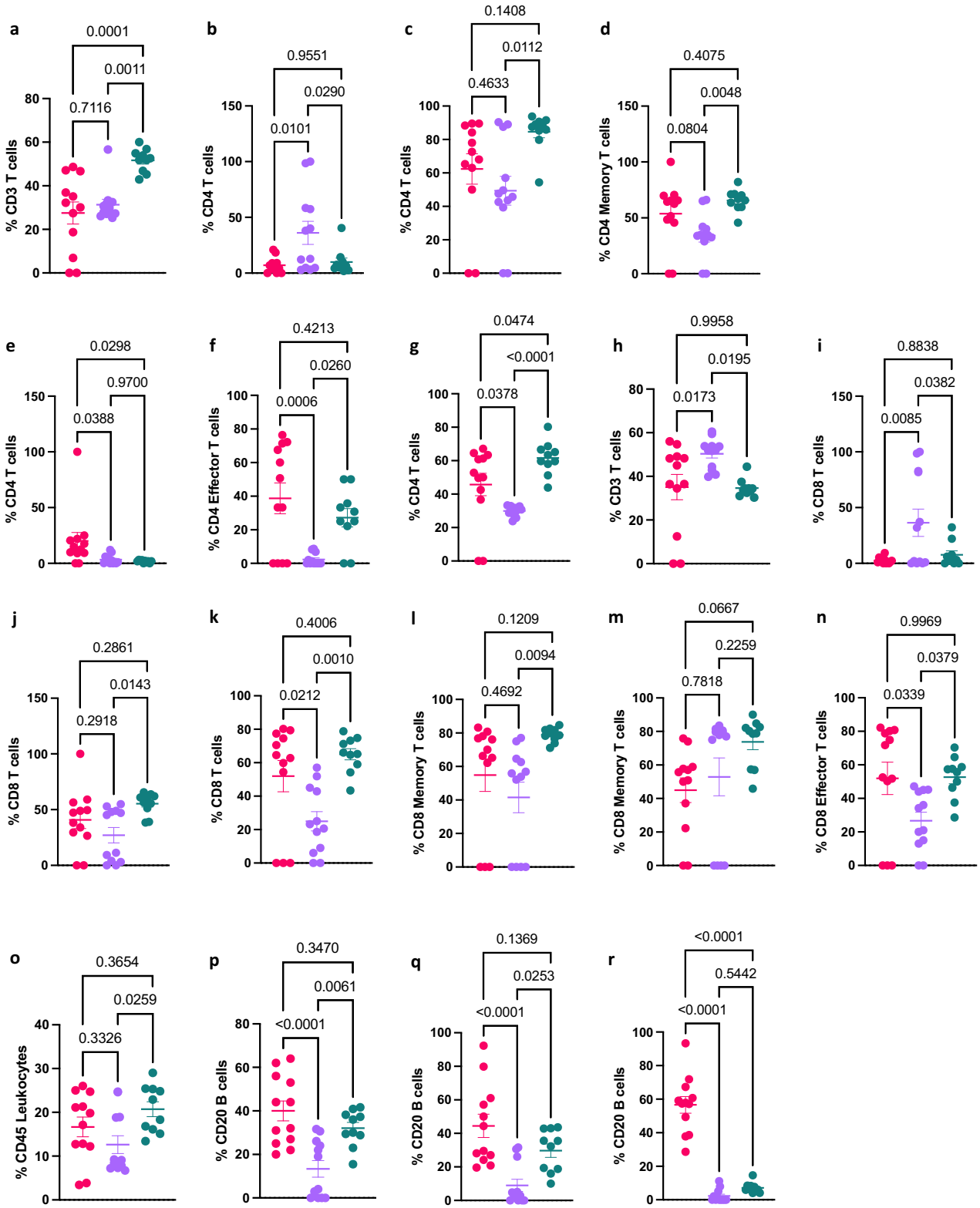

Fig. 8 | Granuloma associated T and B cell profiles. In the three groups of CMs [unvaccinated (strawberry), BCG (lavender)- and *ΔsigH*-vaccinated (teal)], post-*Mtb* infection, shown are the frequencies of lung granuloma derived CD4$^+$ T cells (**a**), expressed as percentage of all CD3$^+$ cells. Frequency of lung granuloma derived naïve (**b**) and memory (**c**) CD4$^+$ T cells, expressed as percentage of the parental population. Within the memory CD4$^+$ T cell pool, shown are the frequencies of CD69$^+$ (**d**) and KI67$^+$ (**e**). Within the effector CD4$^+$ T cell pool, shown is the frequencies of CD69$^+$ (**f**). The frequency of CD69$^+$ (**g**) is also shown for the parental CD4$^+$ T cell pool. Frequencies of lung granuloma derived CD8$^+$ T cells (**h**), expressed as percentage of all CD3$^+$ cells. Frequency of lung granuloma derived naïve (**i**) and memory (**j**) CD8$^+$ T cells, expressed as percentage of the parental population. Frequencies of lung granuloma derived CD8$^+$ CD69$^+$ T cells (**k**), expressed as percentage of parental population. Frequency of lung granuloma derived CD8$^+$ memory CD69$^+$ T (**l**) and CD8$^+$ memory CCR5$^+$ (**m**) T cells, expressed as percentage of the parental population. Frequency of lung granuloma derived CD8$^+$ Effector CD69$^+$ T cells (**n**), expressed as percentage of the parental population. Frequency of lung granuloma derived B cells (**o**) is shown along with CCR5$^+$ (**p**), CD69$^+$ (**q**) and KI67$^+$ (**r**) B cells, expressed as percentage of the parental population. Data is presented as mean ± SEM and *P*-values were calculated by one-way ANOVA with Tukey's correction.

https://doi.org/10.1038/s41467-025-57090-4

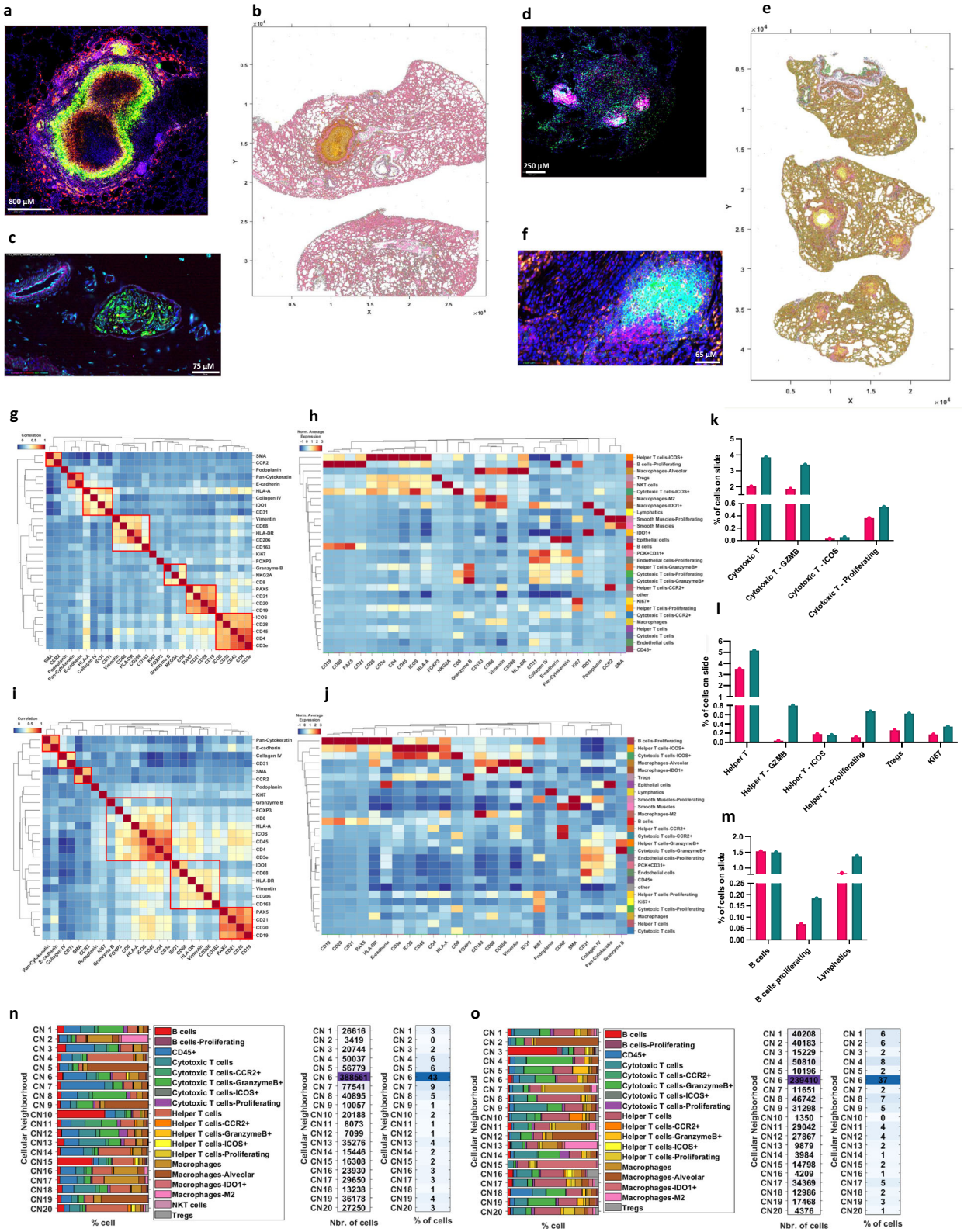

vaccines. rBCG complemented with RD1[55], overexpressing Ag85B[56], or encoding a listeriolysin[57], provide better protection than the parental vaccine. Clearly, live-replicating mycobacterial vaccines have the potential to replace BCG. Attenuated *Mtb* engender more effective T cell responses relative to rBCGs as they express the full complement of *Mtb* antigens, some of which are important for immune recognition[58,59]. Rationally attenuated, live replicating *Mtb* are most likely to afford durable protection, as these express the full complement of protective antigens that are not present in BCG and other classes of vaccines[20]. $CD4^+$ T cell responses to *Mtb* in macaques and humans share antigen dominance, suggesting that vaccines which elicit protection in the former are likely to also protect the latter[18]. Candidates with a track record of safety and efficacy in the relevant NHP model should be prioritized for further development.

Fig. 9 | Comparison of spatial lung granuloma architecture and the impact of *ΔsigH*-vaccination by multiplexed imaging. a CyCIF staining image from a representative lung section from an unvaccinated, *Mtb* challenged macaque, showing staining with the most prominent markers in this group: CD68 - red, HLA-A – pink and HLA-DR - orange, IDO—green and nuclear stain DAPI - blue. **b** Staining of a lung section from the same group with all 27 antibodies. **c** IDO+ (green) cells in this section which do not exhibit the expression of classical myeloid (CD68, CD163, CD206) markers, and which are lineage (CD45) negative, interact with cells positive for structural markers—Collagen IV (pink), E-cadherin (red) and vimentin (cyan). **d** CyCIF staining image from a representative lung section from a *ΔsigH* vaccinated, *Mtb* challenged macaque, showing staining with the most prominent markers in this group: CD20 (pink), CD4 (green), CD19 (pink) and PAX5 (cyan) and nuclear stain DAPI (blue). **e** Staining of the same section with all 27 antibodies. **f** Intense staining of the section with iBALT markers clearly delineates B cell—T cell zones. **g**–**h** Comparative characterization of correlation matrices from CyCIF staining of unvaccinated (**g**) and *ΔsigH* -vaccinated (**h**) lung sections. **i**–**j** Identification of cellular phenotypes based on protein expression results from CyCIF in unvaccinated (**i**) and *ΔsigH* -vaccinated (**j**) lung sections. Frequency of various subpopulations of cytotoxic (**k**) and helper T cells (**l**), B cells (**m**) in unvaccinated (strawberry) and *ΔsigH* -vaccinated (teal) lung sections. Comparison of cellular neighborhoods in unvaccinated (n) and *ΔsigH* -vaccinated (o) lung sections.

Mtb is continuously exposed to stress during its life cycle[60]. Stress-response pathways help *Mtb* survive and persist in the wake of host mechanisms of sterilization. Inactivation of key stress regulators is therefore a potential strategy to generate vaccine candidates. A *Mtb* mutant in stress regulator PhoP[57] is attenuated and efficacious relative to BCG in mice, guinea pigs (GPs) and NHPs and is safe in humans[61–65]. A double knock-out strain of *Mtb* based on this mutant is in advanced clinical testing[66]. Vaccination with *ΔsigE*, another stress response mutant, also protects from *Mtb* infection[67]. Therefore, *Mtb* mutants deficient in the ability to respond to in-vivo stress appear to generate protective immune responses against TB. Our work demonstrates that the inability to scavenge intra-phagocytic or intra-granulomatous redox stress by an *Mtb* strain leads to stronger, protective immune responses. The effectiveness of both *ΔsigH* and MTBVAC, the vaccine candidate containing a deletion in *phoB*, suggests that the pathogen has evolved to interfere with the acquisition of optimal responses to this pathogen. Here we tested the efficacy of the *ΔsigH* mutant, which has already demonstrated a protective phenotype in rhesus, in the cynomolgus macaque model of aerosol infection and provide mechanistic understanding of its effectiveness. Cynomolgus are more resistant to *Mtb* infection, and therefore more closely resemble the human population than rhesus macaques. Our current study thus provides a paradigm towards developing vaccines based on the attenuation of the *Mtb* stress response, that may have the potential to prevent TB disease. These data support the further clinical development of *ΔsigH* for use as a vaccine in humans. Aerosol vaccination with *ΔsigH* focusses protective responses directly at the sites of infection, i.e., the lungs and lung-draining lymph nodes, as opposed to systemically.

SigH regulates responses[9] to multiple stress conditions including phagocytosis, heat-shock[68], nitrosative stress[11], low-pH[13], enduring hypoxia[16] and cigarette smoke[69]. SigH is a bon-a-fide virulence factor of *Mtb* - macaques control infection with the *ΔsigH* in an elite fashion, with significantly reduced lung and extra-thoracic CFU and pathology[18]. Hence, transcriptional programs regulated by SigH are important for *Mtb* to survive in lungs, which is supported by transcript analysis of bacilli recovered from phagocytes[15] and granulomas[70]. Strains of *Mtb* with duplicated *sigH* allele have enhanced pathogenicity of lungs[71]. Similarly, multiplication of *sigH* decreases the protective efficacy of BCG in animal models[72]. Deletion of *sigH* is therefore strongly linked to the development of protective immune responses. Mucosal vaccination with *ΔsigH* protects against lethal TB challenge in rhesus[21,23] as well as cynomolgus macaques (this study) and this protection is significantly better than comparable BCG vaccination. While significant differences were not observed the total lung pathology, including inflammation and necrosis, between the two vaccinated groups due to the use of the resistant cynomolgus model, greater iBALT responses in the *ΔsigH* group contributed to the higher than baseline lung pathology observed in this group. The protected animals were characterized by the presence of strong classical—adaptive (T and B cell) - responses including antigen-specific responses post-vaccination. It should therefore be possible to protect against lethal *Mtb* infection in the setting of human lungs by invoking such classical responses. The inability of *ΔsigH* to scavenge redox stress mounted by infected phagocytes is linked to its inability to prevent phagolysosomal fusion, leading to efficient antigen-presentation, including cross-presentation, likely leading to robust, antigen-specific T cell responses that are protective including MHC I restricted responses. The rapid control of *ΔsigH* relative to *Mtb*[18] likely results in the mitigation of oxidative stress responses. Oxidative stress can enhance cysteine modifications on T cell antigens, impairing intracellular events involved in antigen processing and presentation to T cells[73] and negatively impacting the host immune response[74]. Improved antigen-presentation to T cells during mucosal vaccination with *ΔsigH* results in significantly higher levels of IFNG production by lung $CD4^+$ and $CD8^+$ T cells relative to BCG. The lung environment is thus characterized by optimally balanced protective IFNG responses, with potentially pathogenic Type I IFN responses[75]. In contrast, infection of macaque (and possibly human) lungs with the pathogenic *Mtb* results in over-exuberant Type I IFN production from pDCs, which are efficiently recruited to lung granulomas[28]. This results in contrasting immune responses. Pathogenic *Mtb* induces a primary response with significantly high expression of ISGs and inflammatory genes, amplifying the impact of Type I IFN. This can in turn inhibit IFNG response[75]. Mucosal *ΔsigH* vaccination balances this response in favor of IFNG, resulting in the recruitment of lung homing, activated, proliferating, IFNG-responsive, memory $CD4^+$ and $CD8^+$ T cell responses (Figs. 2–3). Under these conditions IRF8, the expression of which is induced to higher levels by *ΔsigH* vaccination in pDCs (Fig. 5k), can cooperate with BCL6 to induce lymphoid follicles[23]. Such follicles, enriched in B cells, are critical for *ΔsigH*-induced protection against TB[23]. B cells in these follicles enhance cytokine production and strategically localize T(FH)-like cells via interactions between programmed cell death 1 (PD-1) and its ligand PD-L1 and mediate *Mtb* control[23], resulting is even more robust memory T cell responses. The role of IFNG-responsive T cells (T-IFNs), a unique population of T cells, in mediating protection against TB via *ΔsigH* vaccination is clear. Significantly higher induction of IFNG following *ΔsigH* vaccination, and the ensuing recruitment of T-IFNs, as well as proliferative, activated, and cytotoxic T cells to the lungs, is responsible for the activation of IFNG-responsive macrophages in the same compartment, correlating with lower *Mtb* CFUs and pathology (Fig. 1). Thus, our work shows that classical adaptive immune responses – IFNG expressing $CD4^+$ and $CD8^+$ T cells, Th1/Th17 T cells, IFN-responsive T cells, and B-T cell cooperation within lymphoid follicles, correlate with elite protection against TB. Our results also suggest that *ΔsigH* vaccination results in the efficient elicitation of Th1(IFNG/TNF-α) as well as Th17 (IL17) responses, correlating with the control of *Mtb* challenge. T cells exist in a continuum of effector states - resting, activation, IFN-responsive and proliferative[25]. Interpretation of our flow cytometry and scRNAseq results shows that mucosal *ΔsigH* vaccination invokes the recruitment of T cells that are pushed from resting to activated, IFN-responsive and proliferative end of the spectrum. During infection T cells express two major modules: cellular cytotoxicity and cytokine expression[25]. Our results show that mucosal *ΔsigH* vaccination modulates the phenotype of lung T cells (both $CD4^+$ and $CD8^+$) to enhanced cellular cytotoxicity and cytokine expression phenotype.

Despite our promising early results, including the elicitation of protection against TB by *ΔsigH* in two different NHP species, further development of this attenuated strain is needed before it can be used in human trials as a potential anti-TB vaccine[76,77]. Combining mutations to enhance the safety of *Mtb* strains is a proven strategy[78] and recommended by the Geneva Consensus on live-attenuated *Mtb* based TB vaccines[76]. We propose to increase the safety of *ΔsigH* and evaluate if the immunogenicity and efficacy of the parent vehicle is retained by generating multiple double or triple knock outs (DKO, TKO) each of which includes the *ΔsigH* deletion. These strains should progressively be evaluated in-vitro, and in animal models to determine safety relative to the parental strain including in the setting of HIV co-infection. BCG vaccination results in disseminated disease in the HIV infected, particularly infants[79]. Macaques provide a platform to study *Mtb*/HIV co-infection[32,80] including in the presence of ART[81,82]. The *ΔsigH* single KO was completely safe upon SIV co-infection[19], indicating that mutants based on *ΔsigH* may be safe for use in humans. DKO/TKO in the *ΔsigH* must however also be evaluated in the NHP *Mtb*/SIV co-infection model, including in the presence of ART and chronic immune activation. Another potential limitation of our study is that it did not evaluate the durability of protective responses, although we show that protection is mediated by memory T cells, and these responses should prove to be durable. This however remains to be tested. Eventually our proposed studies will generate human-ready live attenuated *Mtb* mutants in *sigH*, via the elicitation of classical, IFNG-producing $CD4^+$ and $CD8^+$ T cell responses which instruct macrophages to limit *Mtb*. Importantly however, mucosal vaccination with *ΔsigH* results in impressive protection observed in the macaque model, comparable to that observed with IV BCG[4]. Interestingly, immune correlates of protection from IV BCG and *ΔsigH* vaccination in macaques appear to be shared[83].

Methods

NHP study design and infections

All procedures adhered to NIH guidelines and received approval from the Institutional Animal Care and Use Committees (IACUC) of Texas Biomedical Research Institute ($n = 15$) or Tulane National Primate Research Center ($n = 10$). 25 mycobacteria-naive cynomolgus macaques (CMs)[84], obtained from the NIAID ($n = 10$) or Envigo, USA ($n = 15$), were used in this study protocol (Table S1). Specifically, the animals were either unvaccinated ($n = 9$) or aerosol vaccinated with 1000 Colony Forming Units (CFUs) of BCG ($n = 7$) or *ΔsigH* ($n = 9$), as described earlier[21]. 8-weeks post-vaccination, macaques were exposed to 100 CFU aerosolized *Mtb* CDC1551 (Fig. 1a). Infection was assessed through tuberculin skin test (TST) or antigen-specific ICS, while TB progression was monitored by longitudinal measurements of weight, temperature, and C-reactive protein (CRP) and bronchoalveolar lavage (BAL) CFUs, and chest X rays (CXR) as described[21,85–88]. Dissemination was evaluated during necropsy by culturing bronchial lymph node, spleen, liver, and kidney tissues to measure CFUs. Demographic information including age, gender, etc., and study specific information of macaques are provided (Table S1). Animals were euthanized at 12–13 weeks post-challenge.

Sampling

TST was performed 1–3 weeks before challenge and at weeks 3 and 5 post-challenge, as described[21,89]. CXR scans were performed one week before *Mtb* infection and 4 weeks post-infection as described[90] and scored in a blinded manner by a board-certified veterinary radiologist. BAL samples were obtained one week before either vaccination or *Mtb* infection and subsequently every two weeks, as described[21,32]. BAL cells were used for determining bacterial burden and cellular analysis through flow cytometry, as described[21,32]. Blood samples were collected one week prior to vaccination or *Mtb* infection and thereafter on a weekly basis, for measuring complete blood count, serum chemistry, including serum C-reactive protein (CRP), and for flow cytometry, employing the flow panels specified in Table S2[32,87,91].

Tissue bacterial burden and pathology

Tissues were collected and processed as described[21]. CFUs were determined per gram of tissue and per mL of BAL fluid. Lung pathology at necropsy was assessed by a board-certified veterinary pathologist in a blinded manner, utilizing zinc-formalin-fixed paraffin-embedded (FFPE) tissues representing all lung lobes using previously described methods[21].

Immune analysis

Different immunocyte populations were quantified and characterized in whole blood, BAL and lungs using flow cytometry, following established protocols[23,28,90,92,93]. T cell populations and their functionality were assessed through stimulations and analyzed using flow cytometry (Table S2, Fig. S10), as detailed in prior publications[21,32,87,94].

Single cell RNAseq

Single-cell RNA sequencing (scRNAseq) was conducted as described[95,96] on BAL cells obtained at pre- and post-vaccination and post-challenge time points. The fastq files were aligned against the *M. fascicularis* reference genome with *cellranger count*. Gene set enrichment analysis was performed using *fgsea*[97] using hallmark pathways for human from *msigdbr*[98] after converting the macaque genes to homologs human genes. Ligand-receptor interaction prediction was performed using *SingleCellSignalR*[99]. Several R packages were used to generate figures and intermediate data preprocessing, such as *ggplot2*[100] and *biomaRt*[101], pheatmap[102] and *stringr*[103].

Spatial multiplexed imaging

CyCIF staining was conducted collaboratively with Akoya Biosciences (Marlborough, MA, USA), following the procedures outlined in previous studies[104]. Antibodies sourced from commercial vendors (Table S3) were conjugated to custom oligo barcodes (#7000009; Akoya). Complementary oligo-conjugated fluorophore reporters were procured from Akoya. FFPE lung section slides were stained overnight with the initial antibody cocktail, comprising the first 28 antibodies and fixed in paraformaldehyde (PN# 15710; Electron Microscopy Sciences). A reporter stock solution was prepared as outlined in the PhenoCycler-Fusion User Guide, incorporating 10X Buffer (#7000019), Assay Reagent (#7000002), and Nuclear Stain (#7000003) from Akoya. Individual tubes containing 3 reporters per cycle were then diluted in the reporter stock solution (Table S3). Subsequently, a 96-well plate was prepared with 1-well/cycle containing the corresponding working reporter solution for that cycle. A flow cell (#240204; Akoya) was assembled onto the slide and PhenoCycler-Fusion (Akoya) used at the following exposure settings: DAPI—1 ms, ATTO550 channel—150 ms, AF647 channel—150 ms, and AF750 channel—150 ms to capture whole slide images of three markers (+ DAPI, nuclear stain) at a time. The final QPTIFF file encompassing a composite image of all markers was examined using the QuPath software (https://qupath.github.io/), with individual or collective toggling of each channel, revealing the spatial expression pattern of the marker(s) of interest. Data was analyzed using Akoya's Multiplexed Image Analysis (MIA) Graphical User Interface, including quality control, filtration, nuclear segmentation[104] and cytoplasm segmentation. To phenotype various cell populations, the mean fluorescent intensity (MFI) of each marker was calculated for each cell, considering the corresponding expression compartment. The normalized MFI expression for all markers (columns) and cells (rows) from each QPTiff image were used for unsupervised clustering with Leiden[105] algorithm and GPU-accelerated[106] methods to assign phenotypes. Dimensionality reduction for data visualization was performed using UMAP and tSNE through the implementations provided by Scanpy[105] and Rapids[106].

Spatial interactions between different cell phenotypes were quantified using the Cellular Neighborhood method[107].

Gene expression in human macrophages and ex-vivo antigen-presentation assay

We investigated the growth and immunogenicity of *ΔsigH* compared to *Mtb* (CDC1551) in human macrophages (HMΦs), using previously described methods[37]. HMΦs obtained from two healthy donors were pooled and three pools per group were infected at MOI = 1. HMΦs were lysed and plated for CFU counts on 7H11 agar at 3, 5, and 7 days post infection. Two pools of HMΦs obtained from three donors each were infected as described above and RNAseq was performed. Data were analyzed using Reactome, KEGG and Gene enrichment sequence analysis (GSEA) workflows (Clusterprofile software, Novogene, USA) to identify multiple differentially expressed genes (DEGs) associated with the regulation of anti-TB immunity, as described[37].

TRIzol (Invitrogen, USA) lysates of preparations described above were used for RT-PCR analysis using primers (Table S4) for *ATG5* (**d**), *ATG7* (**e**), *GBP1* (**f**), GBP2 (**g**) genes.

For ex-vivo antigen-presentation assays, HMΦs derived from two HLA-DR1$^+$ healthy human donors were pooled and three pools were infected with *ΔsigH* and *Mtb* (MOI = 1) for 4 hours. After washing, the cells were overlaid with F9A6 CD4 T cell hybridoma (kindly provided by Prof. David Canaday, CWRU, OH), which secretes IL-2 upon recognizing an epitope of *Mtb* Antigen-85B in the context of HLA-DR1. After 48 and 72 hours, the supernatants were tested for IL-2 using a sandwich ELISA. The kit for human siRNAs (mixture of duplexes), were purchased from Origene (SR322490). Three pools of MΦs were treated with siRNA and the scrambled control according to the manufacturers' instructions, and this was followed by addition of Mtb (H37Rv) for 4 h (MOI of 1). After washing, the cells were overlaid with F9A6 CD4 T cell hybridoma and the supernatants collected after 24 h were tested for IL-2 using a sandwich ELISA.

Reporting summary

Further information on research design is available in the Nature Portfolio Reporting Summary linked to this article.

Data availability

Source data are provided with this paper. All data supporting the findings of this study are available within this manuscript and its Supplementary Information. Any additional data can be requested from the corresponding authors upon reasonable request. The scRNAseq raw data generated in this study have been deposited to the Gene Expression Omnibus- GEO (NCBI) under accession number GSE283562. The RNAseq dataset have been deposited in the NCBI BioProject database under accession number PRJNA1202673. Source data are provided with this paper.

References

1. Bagcchi, S. WHO's global tuberculosis report 2022. *Lancet Microbe* **4**, e20 (2023).
2. Organization, W. H. *Global tuberculosis report 2023*. (Geneva: World Health Organization, 2023).
3. Trunz, B. B., Fine, P. & Dye, C. Effect of BCG vaccination on childhood tuberculous meningitis and miliary tuberculosis worldwide: a meta-analysis and assessment of cost-effectiveness. *Lancet* **367**, 1173–1180 (2006).
4. Darrah, P. A. et al. Prevention of tuberculosis in macaques after intravenous BCG immunization. *Nature* **577**, 95–102 (2020).
5. McShane, H. et al. BCG: myths, realities, and the need for alternative vaccine strategies. *Tuberculosis (Edinb.)* **92**, 283–288 (2012).
6. Kaufmann, S. H. & Gengenbacher, M. Recombinant live vaccine candidates against tuberculosis. *Curr. Opin. Biotechnol.* **23**, 900–907 (2012).
7. Perez, I. et al. Live attenuated TB vaccines representing the three modern Mycobacterium tuberculosis lineages reveal that the Euro-American genetic background confers optimal vaccine potential. *EBioMedicine* **55**, 102761 (2020).
8. Aguilo, N. et al. Reactogenicity to major tuberculosis antigens absent in BCG is linked to improved protection against Mycobacterium tuberculosis. *Nat. Commun.* **8**, 16085 (2017).
9. Mehra, S. & Kaushal, D. Functional genomics reveals extended roles of the Mycobacterium tuberculosis stress response factor sigmaH. *J. Bacteriol.* **191**, 3965–3980 (2009).
10. Kernodle, D. S. SigH, antioxidants, and the pathogenesis of pulmonary tuberculosis. *J. Infect. Dis.* **205**, 1186–1188 (2012).
11. Darwin, K. H., Ehrt, S., Gutierrez-Ramos, J. C., Weich, N. & Nathan, C. F. The proteasome of Mycobacterium tuberculosis is required for resistance to nitric oxide. *Science* **302**, 1963–1966 (2003).
12. Manganelli, R. et al. Role of the extracytoplasmic-function sigma factor sigma(H) in Mycobacterium tuberculosis global gene expression. *Mol. Microbiol* **45**, 365–374 (2002).
13. Rohde, K. H., Abramovitch, R. B. & Russell, D. G. Mycobacterium tuberculosis invasion of macrophages: linking bacterial gene expression to environmental cues. *Cell Host Microbe* **2**, 352–364 (2007).
14. Schnappinger, D. et al. Transcriptional adaptation of Mycobacterium tuberculosis within macrophages: insights into the phagosomal environment. *J. Exp. Med* **198**, 693–704 (2003).
15. Graham, J. E. & Clark-Curtiss, J. E. Identification of Mycobacterium tuberculosis RNAs synthesized in response to phagocytosis by human macrophages by selective capture of transcribed sequences (SCOTS). *Proc. Natl Acad. Sci. USA* **96**, 11554–11559 (1999).
16. Rustad, T. R., Harrell, M. I., Liao, R. & Sherman, D. R. The enduring hypoxic response of Mycobacterium tuberculosis. *PLoS One* **3**, e1502 (2008).
17. Dutta, N. K., Mehra, S. & Kaushal, D. A Mycobacterium tuberculosis sigma factor network responds to cell-envelope damage by the promising anti-mycobacterial thioridazine. *PLoS One* **5**, e10069 (2010).
18. Mehra, S. et al. The Mycobacterium tuberculosis stress response factor SigH is required for bacterial burden as well as immunopathology in primate lungs. *J. Infect. Dis.* **205**, 1203–1213 (2012).
19. Foreman, T. W. et al. Nonpathologic infection of macaques by an attenuated mycobacterial vaccine is not reactivated in the setting of HIV co-infection. *Am. J. Pathol.* **187**, 2811–2820(2017).
20. Dutta, N. K. et al. The stress-response factor SigH modulates the interaction between Mycobacterium tuberculosis and host phagocytes. *PLoS One* **7**, e28958 (2012).
21. Kaushal, D. et al. Mucosal vaccination with attenuated Mycobacterium tuberculosis induces strong central memory responses and protects against tuberculosis. *Nat. Commun.* **6**, 8533 (2015).
22. Gough, M. et al. Peripheral blood markers correlate with the progression of active tuberculosis relative to latent control of mycobacterium tuberculosis infection in macaques. *Pathogens* **11**, 544 (2022).
23. Swanson, R. V. et al. Antigen-specific B cells direct T follicular-like helper cells into lymphoid follicles to mediate Mycobacterium tuberculosis control. *Nat. Immunol.* **24**, 855–868 (2023).
24. Mensali, N. et al. Antigen-delivery through invariant chain (CD74) boosts CD8 and CD4 T cell immunity. *Oncoimmunology* **8**, 1558663 (2019).
25. Szabo, P. A. et al. Single-cell transcriptomics of human T cells reveals tissue and activation signatures in health and disease. *Nat. Commun.* **10**, 4706 (2019).
26. Perng, Y. C. & Lenschow, D. J. ISG15 in antiviral immunity and beyond. *Nat. Rev. Microbiol* **16**, 423–439 (2018).

27. McNab, F., Mayer-Barber, K., Sher, A. & Wack, A. & O'Garra, A. Type I interferons in infectious disease. *Nat. Rev. Immunol.* **15**, 87–103 (2015).
28. Esaulova, E. et al. The immune landscape in tuberculosis reveals populations linked to disease and latency. *Cell Host Microbe* **29**, 165–178 (2020).
29. Mehra, S. et al. Granuloma correlates of protection against tuberculosis and mechanisms of immune modulation by Mycobacterium tuberculosis. *J. Infect. Dis.* **207**, 1115–1127 (2013).
30. McCaffrey, E. F. et al. The immunoregulatory landscape of human tuberculosis granulomas. *Nat. Immunol.* **23**, 318–329 (2022).
31. Gautam, U. S. et al. In vivo inhibition of tryptophan catabolism reorganizes the tuberculoma and augments immune-mediated control of Mycobacterium tuberculosis. *Proc. Natl Acad. Sci. USA* **115**, E62–E71 (2018).
32. Foreman, T. W. et al. CD4+ T-cell-independent mechanisms suppress reactivation of latent tuberculosis in a macaque model of HIV coinfection. *Proc. Natl Acad. Sci. USA* **113**, E5636–E5644 (2016).
33. Lancien, M. et al. Dendritic cells require TMEM176A/B ion channels for optimal MHC class ii antigen presentation to naive CD4(+) T cells. *J. Immunol.* **207**, 421–435 (2021).
34. Mehta, M., Rajmani, R. S. & Singh, A. Mycobacterium tuberculosis WhiB3 responds to vacuolar pH-induced changes in mycothiol redox potential to modulate phagosomal maturation and virulence. *J. Biol. Chem.* **291**, 2888–2903 (2016).
35. Zou, W. et al. Macrophage-derived dendritic cells have strong Th1-polarizing potential mediated by beta-chemokines rather than IL-12. *J. Immunol.* **165**, 4388–4396 (2000).
36. Castiello, L., Arico, E., D'Agostino, G., Santodonato, L. & Belardelli, F. In situ vaccination by direct dendritic cell inoculation: the coming of age of an old idea? *Front Immunol.* **10**, 2303 (2019).
37. Khan, A. et al. Human M1 macrophages express unique innate immune response genes after mycobacterial infection to defend against tuberculosis. *Commun. Biol.* **5**, 480 (2022).
38. Mubeen, S. et al. The impact of pathway database choice on statistical enrichment analysis and predictive modeling. *Front Genet* **10**, 1203 (2019).
39. Singh, C. R. et al. Processing and presentation of a mycobacterial antigen 85B epitope by murine macrophages is dependent on the phagosomal acquisition of vacuolar proton ATPase and in situ activation of cathepsin D. *J. Immunol.* **177**, 3250–3259 (2006).
40. Ramachandra, L. et al. Phagosomal processing of Mycobacterium tuberculosis antigen 85B is modulated independently of mycobacterial viability and phagosome maturation. *Infect. Immun.* **73**, 1097–1105 (2005).
41. Ramachandra, L., Noss, E., Boom, W. H. & Harding, C. V. Processing of Mycobacterium tuberculosis antigen 85B involves intraphagosomal formation of peptide-major histocompatibility complex II complexes and is inhibited by live bacilli that decrease phagosome maturation. *J. Exp. Med* **194**, 1421–1432 (2001).
42. Katti, M. K. et al. The Delta fbpA mutant derived from Mycobacterium tuberculosis H37Rv has an enhanced susceptibility to intracellular antimicrobial oxidative mechanisms, undergoes limited phagosome maturation and activates macrophages and dendritic cells. *Cell Microbiol* **10**, 1286–1303 (2008).
43. Singh, B. et al. Myeloid-derived suppressor cells mediate T cell dysfunction in nonhuman primate TB granulomas. *mBio* **12**, e0318921 (2021).
44. Abid, S. et al. CCR2/CCR5-mediated macrophage-smooth muscle cell crosstalk in pulmonary hypertension. *Eur. Respir. J.* **54**, 1802308 (2019).
45. Shi, J., Hu, C. L., Gao, Y. F., Liao, X. X. & Xu, H. The relationship between platelet endothelial cell adhesion molecule-1 and paraquat-induced lung injury in rabbits. *World J. Emerg. Med* **3**, 60–64 (2012).
46. Woodfin, A., Voisin, M. B. & Nourshargh, S. PECAM-1: a multifunctional molecule in inflammation and vascular biology. *Arterioscler Thromb. Vasc. Biol.* **27**, 2514–2523 (2007).
47. Christofidou-Solomidou, M., Nakada, M. T., Williams, J., Muller, W. A. & DeLisser, H. M. Neutrophil platelet endothelial cell adhesion molecule-1 participates in neutrophil recruitment at inflammatory sites and is down-regulated after leukocyte extravasation. *J. Immunol.* **158**, 4872–4878 (1997).
48. Berman, M. E., Xie, Y. & Muller, W. A. Roles of platelet/endothelial cell adhesion molecule-1 (PECAM-1, CD31) in natural killer cell transendothelial migration and beta 2 integrin activation. *J. Immunol.* **156**, 1515–1524 (1996).
49. Tang, Q. & Hendricks, R. L. Interferon gamma regulates platelet endothelial cell adhesion molecule 1 expression and neutrophil infiltration into herpes simplex virus-infected mouse corneas. *J. Exp. Med* **184**, 1435–1447 (1996).
50. Kilapandal Venkatraman, S. M., Sivanandham, R., Pandrea, I. & Apetrei, C. BCG Vaccination and Mother-to-Infant Transmission of HIV. *J. Infect. Dis.* **222**, 1–3 (2020).
51. Bruffaerts, N., Huygen, K. & Romano, M. DNA vaccines against tuberculosis. *Expert Opin. Biol. Ther.* **14**, 1801–1813 (2014).
52. Doherty, T. M., Dietrich, J. & Billeskov, R. Tuberculosis subunit vaccines: from basic science to clinical testing. *Expert Opin. Biol. Ther.* **7**, 1539–1549 (2007).
53. Hokey, D. A. et al. A nonhuman primate toxicology and immunogenicity study evaluating aerosol delivery of AERAS-402/Ad35 Vaccine: Evidence for transient t cell responses in peripheral blood and robust sustained responses in the lungs. *Hum. Vaccin Immunother.* **10**, 2199–2210 (2014).
54. Ottenhoff, T. H. & Kaufmann, S. H. Vaccines against tuberculosis: where are we and where do we need to go? *PLoS Pathog.* **8**, e1002607 (2012).
55. Pym, A. S. et al. Recombinant BCG exporting ESAT-6 confers enhanced protection against tuberculosis. *Nat. Med* **9**, 533–539 (2003).
56. Horwitz, M. A., Harth, G., Dillon, B. J. & Maslesa-Galic, S. Recombinant bacillus calmette-guerin (BCG) vaccines expressing the Mycobacterium tuberculosis 30-kDa major secretory protein induce greater protective immunity against tuberculosis than conventional BCG vaccines in a highly susceptible animal model. *Proc. Natl Acad. Sci. USA* **97**, 13853–13858 (2000).
57. Hess, J. et al. Mycobacterium bovis Bacille Calmette-Guerin strains secreting listeriolysin of Listeria monocytogenes. *Proc. Natl Acad. Sci. USA* **95**, 5299–5304 (1998).
58. Sambandamurthy, V. K. & Jacobs, W. R. Jr Live attenuated mutants of Mycobacterium tuberculosis as candidate vaccines against tuberculosis. *Microbes Infect.* **7**, 955–961 (2005).
59. Sambandamurthy, V. K. et al. Long-term protection against tuberculosis following vaccination with a severely attenuated double lysine and pantothenate auxotroph of Mycobacterium tuberculosis. *Infect. Immun.* **73**, 1196–1203 (2005).
60. Flentie, K., Garner, A. L. & Stallings, C. L. Mycobacterium tuberculosis transcription machinery: ready to respond to host attacks. *J. Bacteriol.* **198**, 1360–1373 (2016).
61. Perez, E. et al. An essential role for phoP in Mycobacterium tuberculosis virulence. *Mol. Microbiol* **41**, 179–187 (2001).
62. Martin, C. et al. The live Mycobacterium tuberculosis phoP mutant strain is more attenuated than BCG and confers protective immunity against tuberculosis in mice and guinea pigs. *Vaccine* **24**, 3408–3419 (2006).
63. Verreck, F. A. et al. MVA.85A boosting of BCG and an attenuated, phoP deficient M. tuberculosis vaccine both show protective efficacy against tuberculosis in rhesus macaques. *PLoS One* **4**, e5264 (2009).

64. Arbues, A. et al. Construction, characterization and preclinical evaluation of MTBVAC, the first live-attenuated M. tuberculosis-based vaccine to enter clinical trials. *Vaccine* **31**, 4867–4873 (2013).
65. Spertini, F. et al. Safety of human immunisation with a live-attenuated Mycobacterium tuberculosis vaccine: a randomised, double-blind, controlled phase I trial. *Lancet Respir. Med* **3**, 953–962 (2015).
66. Martin, C., Marinova, D., Aguilo, N. & Gonzalo-Asensio, J. MTBVAC, a live TB vaccine poised to initiate efficacy trials 100 years after BCG. *Vaccine* **39**, 7277–7285 (2021).
67. Hernandez Pando, R., Aguilar, L. D., Smith, I. & Manganelli, R. Immunogenicity and protection induced by a Mycobacterium tuberculosis sigE mutant in a BALB/c mouse model of progressive pulmonary tuberculosis. *Infect. Immun.* **78**, 3168–3176 (2010).
68. Raman, S. et al. The alternative sigma factor SigH regulates major components of oxidative and heat stress responses in Mycobacterium tuberculosis. *J. Bacteriol.* **183**, 6119–6125 (2001).
69. Willemse, D., Moodley, C., Mehra, S. & Kaushal, D. Transcriptional response of mycobacterium tuberculosis to cigarette smoke condensate. *Front Microbiol* **12**, 744800 (2021).
70. Hudock, T. A. et al. Hypoxia sensing and persistence genes are expressed during the intragranulomatous survival of mycobacterium tuberculosis. *Am. J. Respir. Cell Mol. Biol.* **56**, 637–647 (2017).
71. Domenech, P., Kolly, G. S., Leon-Solis, L., Fallow, A. & Reed, M. B. Massive gene duplication event among clinical isolates of the Mycobacterium tuberculosis W/Beijing family. *J. Bacteriol.* **192**, 4562–4570 (2010).
72. Sadagopal, S. et al. Reducing the activity and secretion of microbial antioxidants enhances the immunogenicity of BCG. *PLoS One* **4**, e5531 (2009).
73. Preynat-Seauve, O., Coudurier, S., Favier, A., Marche, P. N. & Villiers, C. Oxidative stress impairs intracellular events involved in antigen processing and presentation to T cells. *Cell Stress Chaperones* **8**, 162–171 (2003).
74. Trujillo, J. A. et al. The cellular redox environment alters antigen presentation. *J. Biol. Chem.* **289**, 27979–27991 (2014).
75. Kotov, D. I. et al. Early cellular mechanisms of type I interferon-driven susceptibility to tuberculosis. *Cell* **186**, 5536–5553 e5522 (2023).
76. Kamath, A. T. et al. New live mycobacterial vaccines: the Geneva consensus on essential steps towards clinical development. *Vaccine* **23**, 3753–3761 (2005).
77. Walker, K. B. et al. The second Geneva Consensus: recommendations for novel live TB vaccines. *Vaccine* **28**, 2259–2270 (2010).
78. Hinchey, J. et al. Lysine auxotrophy combined with deletion of the SecA2 gene results in a safe and highly immunogenic candidate live attenuated vaccine for tuberculosis. *PLoS One* **6**, e15857 (2011).
79. Hesseling, A. C. et al. The risk of disseminated Bacille Calmette-Guerin (BCG) disease in HIV-infected children. *Vaccine* **25**, 14–18 (2007).
80. Bucsan, A. N. et al. Mechanisms of reactivation of latent tuberculosis infection due to SIV co-infection. *J. Clin. Invest* **129**, 5254–5260(2019).
81. Ganatra, S. R. et al. Anti-retroviral therapy does not reduce tuberculosis reactivation in a tuberculosis-HIV co-infection model. *J. Clin. Invest* **130**, 5171–5179(2020).
82. Sharan, R. et al. Antiretroviral therapy timing impacts latent tuberculosis infection reactivation in a tuberculosis/simian immunodeficiency virus coinfection model. *J. Clin. Invest.* **132**, e153090(2021).
83. Irvine, E. B. et al. Robust IgM responses following intravenous vaccination with Bacille Calmette-Guerin associate with prevention of Mycobacterium tuberculosis infection in macaques. *Nat. Immunol.* **22**, 1515–1523 (2021).
84. Stammes, M. A. et al. Medical imaging of pulmonary disease in SARS-CoV-2-exposed non-human primates. *Trends Mol. Med.* **28**, p123–142(2021).
85. Lampe, K. et al. Immunization of rhesus macaques with Echinococcus multilocularis recombinant 14-3-3 antigen leads to specific antibody response. *Parasitol. Res.* **116**, 435–439 (2017).
86. Mehra, S. et al. Transcriptional reprogramming in nonhuman primate (rhesus macaque) tuberculosis granulomas. *PLoS One* **5**, e12266 (2010).
87. Mehra, S. et al. The DosR regulon modulates adaptive immunity and is essential for mycobacterium tuberculosis persistence. *Am. J. Respir. Crit. Care Med.* **191**, 1185–1196 (2015).
88. Sharan, R. et al. Isoniazid and rifapentine treatment effectively reduces persistent M. tuberculosis infection in macaque lungs. *J. Clin. Invest* **132**, e161564 (2022).
89. Kaushal, D., Mehra, S., Didier, P. J. & Lackner, A. A. The non-human primate model of tuberculosis. *J. Med Primatol.* **41**, 191–201 (2012).
90. Singh, B. et al. Inhibition of indoleamine dioxygenase leads to better control of tuberculosis adjunctive to chemotherapy. *JCI Insight* **8**, e163101 (2023).
91. Mehra, S. et al. Reactivation of latent tuberculosis in rhesus macaques by coinfection with simian immunodeficiency virus. *J. Med Primatol.* **40**, 233–243 (2011).
92. Bucsan, A. N. et al. Response to hypoxia and the ensuing dysregulation of inflammation impacts mycobacterium tuberculosis pathogenicity. *Am. J. Respir. Crit. Care Med* **206**, 94–104 (2022).
93. Singh, D. K. et al. Responses to acute infection with SARS-CoV-2 in the lungs of rhesus macaques, baboons and marmosets. *Nat. Microbiol* **6**, 73–86 (2021).
94. Phillips, B. L. et al. LAG3 expression in active Mycobacterium tuberculosis infections. *Am. J. Pathol.* **185**, 820–833 (2015).
95. Akter, S. et al. Mycobacterium tuberculosis infection drives a type I IFN signature in lung lymphocytes. *Cell Rep.* **39**, 110983 (2022).
96. Akter, S. & Khader, S. A. A protocol to analyze single-cell RNA-seq data from Mycobacterium tuberculosis-infected mice lung. *STAR Protoc.* **4**, 102544 (2023).
97. Korotkevich, G. et al. Fast gene set enrichment analysis. *Preprint at* http://biorxiv.org/content/early/2016/06/20/060012 (2019).
98. Dolgalev, I. et al. msigdbr: MSigDB gene sets for multiple organisms in a tidy data format. Preprint at https://CRAN.R-project.org/package=msigdbr (2022).
99. Cabello-Aguilar, S. et al. SingleCellSignalR: inference of intercellular networks from single-cell transcriptomics. *Nucleic Acids Res* **48**, e55 (2020).
100. Wickham, H. *Ggplot2: Elegant Graphics for Data Analysis*. (Springer-Verlag New York., 2016).
101. Durinck, S., Spellman, P. T., Birney, E. & Huber, W. Mapping identifiers for the integration of genomic datasets with the R/Bioconductor package biomaRt. *Nat. Protoc.* **4**, 1184–1191 (2009).
102. Kolde, R. et al. pheatmap: pretty heatmaps. *Preprint at* https://cran.r-project.org/package=pheatmap (2019).
103. Wickham, H. et al. stringr: Simple, consistent wrappers for common string operations. *Preprint at* https://cran.r-project.org/package=stringr (2022).
104. Jhaveri, N. et al. Mapping the spatial proteome of head and neck tumors: key immune mediators and metabolic determinants in the tumor microenvironment. *GEN Biotechnol.* **2**, 418–434 (2023).
105. Wolf, F. A., Angerer, P. & Theis, F. J. SCANPY: large-scale single-cell gene expression data analysis. *Genome Biol.* **19**, 15 (2018).
106. Nolet, C. et al. Accelerating single-cell genomic analysis with GPUs. *Preprint at bioRxiv*, https://doi.org/10.1101/2022.05.26.493607 (2022).
107. Schurch, C. M. et al. Coordinated cellular neighborhoods orchestrate antitumoral immunity at the colorectal cancer invasive front. *Cell* **182**, 1341–1359.e1319 (2020).

Acknowledgements
This research was supported by NIH grants AI185028, AI134240, AI138587, AI111914, institutional NIH grants– OD011133, OD010442, OD032443, OD028732, AI161943, AI168439, OD028653 and OD028732. The content is solely the responsibility of the authors and does not necessarily represent the official views of the National Institutes of Health. We are especially grateful to Dr. Larry S. Schlesinger for critical reading and suggestions on draft manuscripts. We also thank Akoya Biosciences and Dr. Yue Hou for supporting the spatial multiplexed imaging through their Spatial Tissue Exploration Program (STEP).

Author contributions
D.K., S.A.K., S.M., D.K.S. and C.J. designed the study; D.K.S. conducted research and data analysis; M.A., S.A., A.N.B., A.M., V.S., N.A.G., P.J.D., E.J.D., Jr., L.A.D., S.H.-U., C.J.R., G.A., S.M. and C.J. contributed to research and/or analyzes; DK wrote the paper with help from D.K.S., S.M., C.J. and S.A.K. All authors contributed to, edited, and approved the manuscript. D.K., S.A.K., S.M., and C.J. provided funding.

Competing interests
All authors declare no competing interests.

Additional information
Supplementary information The online version contains supplementary material available at https://doi.org/10.1038/s41467-025-57090-4.

Correspondence and requests for materials should be addressed to Shabaana A. Khader or Deepak Kaushal.

Peer review information *Nature Communications* thanks William Jacobs, Jialou Zhu and the other, anonymous, reviewer(s) for their contribution to the peer review of this work. A peer review file is available.